Independent roles of *Drosophila* Moesin in imaginal disc morphogenesis and hedgehog signalling

Cristina Molnar and Jose F. de Celis*

Centro de Biología Molecular "Severo Ochoa". CSIC and Universidad Autónoma de Madrid. Cantoblanco. Madrid 28049. Spain

*Author for correspondence: Email: jfdecelis@cbm.uam.es

Phone: 34-91-4974129

Fax: 34-91-4978632

Running title: Moesin role in hedgehog signalling and epithelial morphogenesis.

Key words: Moesin, Hedgehog signalling, epithelial morphogenesis, pattern formation.

Abstract

The three ERM proteins (Ezrin, Radixin and Moesin) form a conserved family required in many developmental processes involving regulation of the cytoskeleton. In general, the molecular function of ERM proteins is to link specific membrane proteins to the actin cytoskeleton. In *Drosophila*, loss of *moesin* (*moe*) activity causes incorrect localisation of maternal determinants during oogenesis, failures in rhabdomere differentiation in the eye and alterations of epithelial integrity in the wing imaginal disc. Some aspects of Drosophila Moe are related to the activity of the small GTPase RhoA, because the reduction of RhoA activity corrects many phenotypes of *moe* mutant embryos and imaginal discs. We have analysed the phenotype of *moesin* loss-of-function alleles in the wing disc and adult wing, and studied the effects of reduced Moesin activity on signalling mediated by the Notch, Decapentaplegic, Wingless and Hedgehog pathways. We found that reductions in Moesin levels in the wing disc cause the formation of wing-tissue vesicles and large thickenings of the vein L3, corresponding to breakdowns of epithelial continuity in the wing base and modifications of Hedgehog signalling in the wing blade, respectively. We did not observe any effect on signalling pathways other than Hedgehog, indicating that the *moe* defects in epithelial integrity have not generalised effects on cell signalling. The effects of *moe* mutants on Hedgehog signalling depend on the correct gene-dose of *rhoA*, suggesting that the requirements for Moesin in disc morphogenesis and Hh signalling in the wing disc are mediated by its regulation of RhoA activity. The mechanism linking Moesin activity with RhoA function and Hedgehog signalling remains to be elucidated.

1. Introduction

Moesin (Moe) is the only member of the Erxin-Radixin-Moesin (ERM) protein family found in *Drosophila*. ERM proteins are involved in many aspects of development, including the control of polarity, cytoskeleton organization, cell adhesion and motility (Bretscher et al., 2000; Bretscher et al., 2002; Louvet-Vallee, 2000; Polesello and Payre, 2004). These proteins are characterised by a N-terminal domain that interacts with specific transmembrane proteins and a C-terminal domain that binds F-actin. The C- and N-terminal domains of ERM proteins are connected by a α-helical region, which allows intramolecular interactions that inactivate the protein (Bretscher et al., 1997; Gary and Bretscher, 1995; Pearson et al., 2000). The protein adopts an open configuration upon binding of phosphatidylinositol 4,5-bisphosphate [PtdIns(4,5)*P*2] and phosphorylation of a threonine residue located in the C-terminal region (Huang et al., 1999; Oshiro et al., 1998; Yonemura et al., 2002; Yonemura and Tsukita, 1999). This open configuration allows interactions between ERM proteins and their heterotypic partners and triggers re-localisation of the protein to the cell membrane (Bretscher, 1999; Tsukita and Yonemura, 1999). Cell culture experiments indicate that ERM proteins link transmembrane proteins to the actin cytoskeleton (Bretscher et al., 1997). These approaches have also uncovered a variety of ERM-interaction partners in different cell types, as well as the existence of cross-interaction with Rho signalling (Ivetic and Ridley, 2004). Thus, ERM proteins associate directly with cell adhesion molecules such as CD44, ICAM-1/2/3 and CD43 (Ivetic and Ridley, 2004). ERMs also bind indirectly, via the adaptor protein EBP50, to other membrane proteins, such as Na^+-H^+-exchanger type 3, the cystic fibrosis transmembrane conductance regulator and the apical determinant Crumbs (Barreiro et al., 2002; Baumgartner et al., 2004; Hamada

et al., 2000; Hamada et al., 2003; Ingraffea et al., 2002; Reczek et al., 1997).

That Moesin is the only ERM in *Drosophila* makes it a model organism to analyse the function of this family of proteins in vivo (Polesello and Payre, 2004). Many developmental roles of *moe* have been described in *Drosophila*, including rhabdomere formation in the eye (Karagiosis and Ready, 2004), regulation of cell shape and polarity during oogenesis (Jankovics et al., 2002; Polesello et al., 2002) and the maintenance of epithelial integrity during imaginal disc development (reviewed in Polesello and Payre, 2004). The rescue of epithelial development of *moe* mutant flies in a *rhoA* loss-of-function background suggests that Moe regulates epithelial integrity by antagonizing RhoA activity, rather than acting as a direct structural component (Speck et al., 2003).

It is unknown whether *moe* is required for signalling events involving the localisation of transmembrane ligands and receptors to particular membrane domains, or membrane recycling processes in the cytoplasm. For example, both the Delta (Dl) ligand and Notch (N) receptor show the same apical localisation (Fehon et al., 1991) as that described for Moe in the wing disc (McCartney and Fehon, 1996). Similarly, the apical region is where the Hedgehog (Hh) binding triggers internalisation of Ptc from the cell surface (Martin et al., 2001; Strutt et al., 2001; Torroja et al., 2004; van den Heuvel, 2003) making the recycling of Ptc a potential site for action of Moe. In addition, the transmembrane protein Smoothened (Smo) accumulates at the basal cell surface upon binding of Hh to Ptc (Denef et al., 2000, van den Heuvel, 2003). This process requires phosphorylation of Smo and it is necessary for Hh signal transduction (Apionishev et al., 2005; Denef et al., 2000; Jia et al., 2004; Lum and Beachy, 2004;

Nakano et al., 2004; Zhang et al., 2005; Zhu et al., 2003). It is not known whether the correct membrane localisation of the Dl, Notch, Ptc and Smo proteins requires Moe function.

We have studied the requirements of *moe* during wing development and imaginal disc morphogenesis. By using a novel *moe* loss-of-function allele, we find that a reduction in Moe levels cause a severe thickening of the L3 vein. The effects of stronger *moe* alleles including the loss of intercellular junctions, disruption of epithelial polarity, cell death and the basal extrusion of cells from the wing epithelium (Speck et al., 2003; Hipfner et al., 2004), do not easily explain this phenotype. We therefore describe the morphology of *moe* mutant wing discs in some detail, using both basal and apical epithelial markers. When Moe expression is reduced, the wing blade epithelium becomes flatter and the basal lamina is distorted, but cells retain their apico-basal polarity. The epithelial folds linking the wing blade and the peripodial membrane, however, show abnormal morphology, epithelial lesions and apoptotic cells. In addition, high-level Hh signalling is compromised in the wing blade, leading to a failure to express normal levels of *ptc* at the anterior-posterior compartment boundary. In contrast, low-level Hh signalling is increased in *moe* mutants, causing the expansion of the L3 vein. The effects of *moe* on Hh signalling depend on the activity of RhoA, as it was described for its requirement in epithelial integrity (Speck et al, 2003). We suggest that Moe contributes to Hh signalling independently of its requirement for epithelial morphology, because the activity of other signalling pathways is not affected by reduced *moe* expression.

2. Results

2.1. Wing phenotypes caused by alterations in moesin function

Several alleles of *moe* cause larval lethality and their developmental effects have been studied in imaginal discs (Speck et al., 2003; Hipfner et al., 2004). The analysis of lethal *moe* alleles in the wing disc uncovered a requirement for the gene in the maintenance of intercellular junctions, epithelial polarity and the correct organisation of actin fibres (Speck et al., 2003; Hipfner et al., 2004). We isolated a novel *moe* loss-of-function allele (moe^{c858}) in a genetic screen designed to identify genes affecting vein patterning when over-expressed (C. Molnar and J.F. de Celis unpublished). Adult flies homozygous for moe^{c858} are viable, the males are fertile, and the females are sterile, most likely due to the requirements of Moe during oogenesis (Jankovics et al., 2002; Polesello et al., 2002).

The moe^{c858} wings are small, distorted and reduced in length. The hinge region is also malformed and reduced in size. In addition, the venation pattern is abnormal and vesicles of wing tissue are localised between the dorsal and ventral wing surfaces (Fig. 1A-E, G-H, I-J). The vesicles differentiate trichomes characteristic of the wing hinge and blade regions (Fig. 1I-J). The vein pattern alterations affect mainly the L3 vein, which forms rings of vein tissue, or is severely thickened (Fig. 1K-M). These venation defects cannot be easily explained by a role of *moe* in maintaining epithelial integrity, but suggest a requirement of *moe* in the mechanisms positioning the L3 vein. The reduction in size observed in *moe* mutant wings is caused in part by a 1.4 times increase in cell density (Fig. 2). Interestingly, when the size of different wing regions is compared in wild type and *moe* wings, the main contribution to cell number reduction

occurs in the L3/L4 intervein (Fig. 2). Thus not only the patterning of the L3 vein but also the distance between the L3 and L4 veins is affected in *moe* mutant wings.

The moe^{c858} mutant phenotypes are variable and affect only a fraction of the mutant flies (Fig. 1B-C; Table 1). This suggests that moe^{c858} is a hypomorphic allele and that the reduction of Moe activity in this mutant may be close a critical threshold to cause a mutant phenotype. To confirm that moe^{c858} is a loss-of-function allele, we made genetic combinations between moe^{c858} and null, or strong hypomorphic, alleles (Karagiosis and Ready, 2004; Polesello et al., 2002; Speck et al., 2003). All allelic combinations display the same phenotypes as the novel moe^{c858} allele; the only detectable difference is in the frequency and severity of the mutant phenotype (Fig. 1D-E and Table 1). To rank alleles quantitatively, we subdivided the mutant phenotypes into two categories ("L3 defects" and "vesicles") and assigned numbers 1 (weaker phenotype) to 3 (stronger phenotype) within each category. The phenotype of moe^{c858} is similar to that caused by expression of *moe RNAi* in the wing blade and hinge (*638-Gal4/UAS-moe RNAi*; Figure 1F) and this phenotype is rescued by over-expression of *moe* in the wing disc (in moe^{c858}*; sal-Gal4/+* males; Table 1). Interestingly, the elimination of one copy of *rhoA* in moe^{c858} males rescues both the "vesicles" phenotype and the "L3 defects" (Table 1). A similar rescue is observed in the case of the stronger allele moe^{PL106}, and the surviving males moe^{PL106}*; rhoA/+* have smaller than normal wings with a normally positioned L3 vein (data not shown). These observations suggest that the wing tissue vesicles and the L3 thickening observed in *moe* wings are caused by inappropriate activity of the small GTPase RhoA.

The allele *moe*^{c858} is caused by the insertion of a P[GS] element (Toba et al., 1999) in the 5' UTR region of the *moe* transcript, corresponding to the exon 1b of Polesello et al. (2002) (Fig. 3A). The insertion site of *moe*^{c858} is very close to the position of other lethal *moe* alleles, and they all map in a 240 bp interval (Fig. 3B). To further characterise the effects of the *moe*^{c858} insertion, we studied the expression of *moe* mRNA and protein in mutant *moe*^{c858} wing discs. We found that the level of the mRNA is reduced in mutant compared to wild type discs (Fig. 3C-D). A similar reduction in *moe* mRNA was observed in *moe*^{PL106} discs (Fig. 3E). In addition, the expression of Moe protein is reduced in *moe*^{c858} discs (Fig. 3F-G). In conclusion, the phenotypes described for *moe*^{c858} correspond to a hypomorphic allele that retains enough Moe function to allow imaginal development and adult viability. In what follows, we will focus our analysis on the effects that reducing *moe* activity has on epithelial morphology and vein patterning.

2.2. Morphology and cell fate in wing imaginal discs mutant for moesin

The appearance of wing-tissue vesicles and the differentiation of a thickened L3 vein in *moe*^{c858} wings, are not easily reconciled with the basal extrusion of imaginal cells from the epithelium and the appearance of apoptotic cells underlying the disc epithelium (Speck et al., 2003; Hipfner et al., 2004). For this reason, we will first describe the morphology of *moe* mutant discs in comparison to wild type discs. This description is necessary to analyse any possible requirement of Moe in cell signalling affecting the positioning of the L3 vein.

The wild type wing disc is a sac of epithelial cells. The cells forming the wing blade and thorax form a columnar epithelium, while the cells in the peripodial

membrane are flatter and form a squamous layer (Fig. 4A and G). The wing epithelium in the mature disc has several folds separating the prospective wing appendage from the peripodial epithelium (Fig. 4A and G). These folds give raise to the wing hinge and pleura in the adult. By staining simultaneously for apical or basolateral epithelial markers, such as Armadillo (Arm), Discs large (Dlg), Fasciclin III (FasIII) or Scribble (Scrib) and basal markers, such as LamininA (LanA), it is possible to follow the pattern of folds and the structure of the epithelium in Z-sections. The apical-basal organisation of moe^{c858} wing cells appears normal (Fig. 4B-C and data not shown). However, the cells in the wing blade appear more flattened in moe^{c858} discs compared to wild type cells; the basal lamina carries lesions and is disorganised, particularly in the wing hinge region (Fig. 4B-C). In a fraction of moe^{c858} mutant discs, folds located underneath the centre of the disc give a multi-layered appearance in transverse sections (Fig. 4B-C, H-I).

We also studied another lethal allele of *moe* (moe^{PL106}) and wing discs in which *moe* activity is reduced by *RNAi* expression (*638-Gal4/UAS-moe RNAi*). In *638-Gal4/UAS-moe RNAi* discs we found similar defects to those described for moe^{c858} discs (Fig. 5E-F, H-I). The pattern of folds is severely disturbed, although the apical-basal organisation of the cells remains normal despite alterations in the basal lamina (Figure 5E-F, H-I). The wings of *638-Gal4/UAS-moe RNAi* flies are similar to the strong moe^{C858} phenotype (Fig. 1C and F). The defects observed in the hinge region of moe^{PL106} discs were in general more extreme that in moe^{c858} and *638-Gal4/UAS-moe RNAi*. Thus, the epithelial structure and basal lamina is much more affected, and the apical expression of epithelial markers is severely modified in the hinge region of moe^{PL106} discs (Fig. 5B-H). The general structure of moe^{PL106} disc becomes progressively

disorganised during growth. Early third instar discs show a more normal appearance that mature discs (Fig. 5). Alterations in both the basal lamina and the distribution of Arm are, however, already detected in early third instar discs (Fig. 5B-C). In all cases, reduction in Moe expression causes cell death in the wing base region, where epithelial integrity is most affected (Fig. 4D for moe^{c858} and supplementary Figure 1 for moe^{PL106}).

Cell fates in moe^{c858} discs with abnormal shape were studied monitoring the expression of genes expressed in the wing blade (Vestigial; Fig. 6A, K), the centre of the wing blade (Spalt; Fig. 6B, O), the wing hinge (Homothorax; Fig. 6C, Q), the wing blade and hinge (Nubbin; Fig. 6D, S), the posterior compartment (Engrailed; Fig. 6E) and the wing margin and hinge (Wingless; Fig. 6B, M). We find that the distribution of cell fates in moe^{c858} mutant discs is identical to that of wild type discs (Fig. 6F-J'). The only change in cell fate we could observe is an expansion in the dorsal region of the wing hinge, detected as an enlarged distal ring of *wingless* expression (Fig. 6G, N). We do not know what causes ectopic *wg* expression in the hinge region of moe mutant wing discs. It could be related to the massive cell death observed in this territory, as detected by activated Cas3 expression, because cell death can cause inappropriate expression of wg (Pérez-Garijo et al., 2004; Pérez-Garijo et al., 2005). Alternatively, moe might participate in some of the mechanisms regulating wg expression in the hinge (Rodríguez del Alamo et al., 2002). It is known that ectopic expression of *wingless* in the wing hinge causes its overgrowth (Klein and Martínez-Arias, 1998; Giraldez and Cohen, 2003), suggesting that the response to Wingless in the hinge region of *moe* discs is normal.

Although cell fates are allocated correctly in *moe*^{c858} mutant discs, the abnormal growth and folding of the disc displaces cells close to the hinge below the wing epithelium (Figure 6F-J, see Z-sections). This change is particularly clear in the proximal region of *spalt* expression and the posterior-most region of the *engrailed* domain, giving an apparent reduction in the size of these domains (Fig. 6G,P and 6J,J'). Nuclei expressing Vestigial or Spalt were observed with a low frequency apparently exiting the epithelium basally (Fig. 6F, G; see also Hipfner et al., 2004; Speck et al., 2003).

Taken together, our observations indicate that when *moe* expression is reduced the morphology of the wing disc is severely affected. The wing blade is flattened, disc folds grow abnormally large and the basal lamina is broken. The most abnormal regions are the disc folds corresponding to the presumptive wing base and hinge. This region also shows epithelial lesions and expresses activated Cas3. There is a good correspondence between the defects observed in the wing hinge of adult *moe*^{c858} flies (Fig. 2E), the presence of wing-hinge vesicles and the abnormal morphology of *moe*^{c858} discs. Interestingly, the distribution of cell fates in the disc and the apico-basal polarity of the wing blade remain normal, suggesting that patterning proceeds correctly in *moe*^{c858} discs despite their morphological alterations.

2.3. Effects of Moesin in cell signalling

The effects of *moe* loss-of-function on vein patterning suggest a requirement of the gene in the positioning of the veins that might be independent of its role in epithelial morphogenesis. Several signalling pathways are involved in the specification of vein territories and their differentiation (de Celis, 2003). The phenotype of *moe* mutant

wings is mainly observed in the vein L3, and consists in variable degree of L3 duplication and thickening (see Fig. 1). In addition the L3/L4 intervein is more reduced in size than other intervein territories, and the distance between L3 and L4 in number of cells is reduced (Fig. 2). These phenotypes indicate a requirement of Moe in the correct specification of the vein L3 and the L3/L4 intervein. Hh signalling directs the formation of the vein L3 and the spacing between the veins L3 and L4 (Gómez-Skarmeta and Modolell, 1996; Mullor et al., 1997). Thus, the patterning phenotypes of loss of *moe* suggest a specific requirement of the gene to regulate the levels and extent of the Hh domain of signalling. We could not detect other phenotypes, such as loss or thickening of longitudinal wing veins, defects in the wing margin and ectopic or loss of sensory elements, which might suggest requirements for *moe* to facilitate the Dpp, Wg, or Notch signalling pathways. Furthermore, the expression of target genes of the Dpp (Phosphorylated Mad, PMad, and Spalt), Wingless (Distalless and Ventral veinless) and Notch (Wingless, Cut) signalling pathways are not affected in moe^{c858} mutant discs (Fig. 6B-G and Fig. 7). These observations also indicate that cell-to-cell communication in the wing blade is not affected non-specifically, implying that the effect of Moe on Hh signalling is not an indirect consequence of alterations in disc morphology and epithelial integrity.

2.4. Effects of Moesin in hedgehog signalling

The Hh signalling pathway regulates gene expression patterns in the anterior central part of the wing disc, corresponding to the territory reached by Hh produced in the posterior compartment. In anterior cells, binding of Hh to its receptor Ptc is associated with phosphorylation of Smo and its accumulation in the cell membrane (Apionishev et al., 2005; Jia et al., 2004). Smo activity inhibits the proteolytic processing of Cubitus

interruptus (Ci) and promotes the formation of a transcriptional activator form of Ci through the inhibition of Suppressor of fused (Lum and Beachy, 2004). In cells not exposed to Hh, the Ci protein is constitutively processed into a 75KD fragment that localises to the nucleus and acts as a transcriptional repressor. Once proteolysis is inhibited, the Ci protein accumulates in the cytoplasm as a 155KD form, which also acts in the nucleus as a transcriptional activator (Bijlsma et al., 2004). The induction of Hh-target expression reflects the existence of low- and high-response thresholds. Consequently, the expression of *ptc*, *engrailed* (*en*) and *knot* (*kn*) is induced by high levels of Hh signalling, while the expression of *dpp* and the *Iroquois* genes (*iro*) is induced by low levels of signalling (Crozatier et al., 2003). The increase in *ptc* expression occurring as a response to Hh signalling is of paramount importance to determine the extent of the Hh domain of signalling, because Ptc accumulation limits the spreading of Hh into the anterior compartment (Chen and Struhl, 1996). Although many biochemical details of Hh signalling are unknown, transmembrane localization and intracellular trafficking of proteins play major roles in regulating the levels of signalling activity and the size of Hh-targets expression domains.

To visualise whether Hh-target gene expression is altered when *moe* function is reduced, we studied the expression of several Hh-target genes in the wing disc. We concentrated our analysis on the wing blade, because the epithelial organisation of this territory is not severely affected in *moe* mutants. The expression of Ptc, a target for high levels of Hh signalling, is reduced in the anterior-posterior compartment boundary of moe^{c858} and moe^{PL106} discs (Fig. 8A-C). Both the width of the stripe of Ptc accumulation is narrower, and the level of expression is lower in mutant than in wild-type discs (Fig. 8A-C). The expression of the gene *ptc*, monitored by a *P-lacZ* insertion

in the gene, is also reduced in *moe* discs compared to wild type ones (Fig. 8D,D'). The expression domains of Engrailed (En) and Knot (Kn) in the anterior compartment are also affected in moe^{c858} mutant discs. The anterior expression of En is very reduced (Fig. 8M-N), while the width of the stripe of Kn expression, is also reduced (Fig. 8E-G, I-K). The reduction of Ptc, En and Kn domains of expression indicates that high levels of Hh signalling are compromised in *moe* mutant discs. The frequency of discs showing defects in Ptc and Kn accumulation (56% of moe^{c858} discs) is higher than the frequency of wings showing patterning defects in the L3 vein and L3/L4 intervein. As expected from the normal appearance of moe^{c858} and moe^{PL106} wings in a *rhoA* heterozygous background ($rhoA^{P1}$/+ and $rhoA^{P2}$/+), the expression of Ptc is not noticeable modified in the corresponding imaginal discs (Supplementary Figure 1).

We also studied the expression of *dpp*, Ci and Caupolican (Caup), which correspond to Hh-target genes activated by low levels of Hh signalling. In all cases we find a moderate expansion of their domains of expression (Fig. 8). Thus, the stripe of Ci maximal accumulation in the anterior compartment (Fig. 8E-F, I-J), the domain of Caup expression in the presumptive L3 (Fig. 8G-H, K-L), and the stripe of *dpp* expression (Figure 8O-P), are broader in moe^{c858} discs that in wild type ones (see summary in Fig. 9F-G). These observations suggest that low-levels of Hh signalling operate in an expanded territory upon a reduction of *moe* expression. The expansion of the domain where low levels of Hh signalling are effective may be a direct consequence of a reduction in *moe* expression. Alternatively, this expansion might be caused by the failure to express *ptc* at normal levels, because a reduction in Ptc is known to result in Hh reaching more anterior cells due to a failure in sequestering Hh (Chen and Struhl, 1996). We notice that reducing Moe levels in the *ptc* domain of expression (in

ptcGal4/UAS-moeRNAi flies) does not affect the extent of the L3 vein, suggesting a direct contribution of *moe* in generating the low-threshold domain of activity (Supplementary Figure 2). The observed expansion of *dpp* expression explains why the Dpp targets *sal* and P-Mad are expressed in a broader territory in *moe* mutant than in wild type discs.

There is a reported interaction between Moe and Ptc proteins in two-hybrid experiments (PimRyder database, Hybrigenics SA at https://pim.hybrigenics.com/prv31/cdsviewer/flybase.jsp). Consequently, we studied in the wing disc the subcellular localisation of Ptc and Moe proteins. The bulk of Moe is detected in the cell's apical side, whereas Ptc is mainly distributed in intracellular vesicles and lateral membrane (Speck et al., 2003; Torroja et al., 2004; see Fig. 9A-B). Thus, the apical accumulation of Moe appears complementary to the membrane expression of Ptc in the sub-apical region of the epidermal cells (Fig. 9B). Clear co-localisation of Ptc and Moe is only detected in moe^{c858} mutant cells located underneath the epithelium (Fig. 9E). In moe^{c858} discs the Ptc localisation appears normal, although the intracellular levels of Ptc are greatly reduced (Fig. 9C-D). The involvement of Moe in Hh signalling was also studied in combinations where the genetic dose of different Hh pathway components is reduced in a moe^{c858} mutant background. We found that only the reduction of the *smo* dose increases the frequency of "strong" L3 phenotypes (Fig. 9H). The reduction of *ptc*, Dpp or its receptor Thick veins does not modify the expressivity of moe^{c858} vesicles nor L3 defects phenotypes (Fig. 9H and data not shown). These observations suggest a specific requirement for Moe in modulating high levels of Hh signalling. The generation of low levels of Hh signalling are not affected upon a reduction of *smo* dose in moe^{c858} wings.

3. Discussion

ERM proteins link transmembrane proteins to the cortical actin cytoskeleton and regulate cytoskeleton dynamics in processes such as microvillar-formation, cell-cell adhesion, maintenance of cell shape, cell motility and membrane trafficking (Bretscher et al., 1997). The single Drosophila ERM protein Moesin promotes cortical actin assembly and apical-basal polarity in the wing disc (Speck et al., 2003). The epithelial lesions and abnormal folding seen in *moe* mutant discs are rescued by a reduction of RhoA activity implying that Moe regulates cell-signalling events that affect actin organization and polarity (Hipfner et al., 2004; Speck et al., 2003). We isolated a novel *moe* allele, moe^{c858}, which allowed us to further analyse the requirements of the gene during imaginal disc morphogenesis and patterning. We were able to define several phenotypes in imaginal wing discs and adult wing structures that indicate additional functions of *moe* in morphogenesis and Hh signalling. These functions also appear to be exerted through the regulation of RhoA activity by Moe.

3.1. Wing disc morphogenesis and epithelial integrity are compromised in moe mutants

In moe^{c858} wings vesicles of wing tissue differentiate between the dorsal and ventral wing surfaces. These vesicles represent groups of cells that leave the epithelium, becoming trapped between the dorsal and ventral wing surfaces after metamorphosis. The vesicles in moe^{c858} wings can be interpreted as a result of the epithelial defects observed in wing discs of other *moe* alleles, in which wing-blade cells leave the basal epithelial surface (Hipfner et al., 2004; Speck et al., 2003). We confirm

that wing cells leave through the basal membrane in *moe*^{c858} discs. The identity of most vesicles, however, corresponds to wing-hinge rather than wing-blade tissue. The hinge region also shows more epithelial lesions and activated Cas3 than the wing pouch. Taken together, these results imply that the hinge region is the most sensitive to lack of Moe activity in *moe*^{c858} mutants, and that groups of cells in the wing hinge loss their continuity with the disc epithelium and remain in contact through the basal membrane.

The morphology of *moe* wing discs is severely disrupted. The wing-blade epithelial cells are abnormally flattened and the altered folding pattern modifies the appearance of the expression domains of cell fate markers. We suggest that the abnormal folding reflects the requirement of Moe to maintain correct apical-basal cell shape. In mutant discs, cells become flattened causing expansion of the folds that now lie underneath the wing blade. A requirement of Moe in maintaining cell shape might be related to the organisation of the F-actin cortical network (Polesello et al., 2002). Several abnormalities in the distribution of apical markers and the formation of the basal lamina were also detected in *moe* mutant discs. The main alteration in *moe* discs is in the structure of the basal lamina, where we show that the expression of LanA is abnormal. Again, the region more affected is the presumptive wing hinge, co-incident with territories where the most expression of activated Cas3 is detected. The suppression of ERM expression in mouse epithelial cells leads to loss of cell-substrate adhesion (Takeuchi et al., 1994). The same result was obtained with two human colo-rectal cancer cell lines in which Ezrin expression is inhibited (Hiscox and Jiang, 1999). Our data support an important function of *moe* in tissue morphogenesis through the generation and/or maintenance of the basal lamina in the wing disc.

3.2. Function of Moe in Hh signalling

A second aspect of *moe* function in the wing disc is its requirement for the patterning of the central region of the wing. The patterning of this territory depends on Hh signalling (Crozatier et al., 2003). Thus, high Hh levels determine the development of the L3/L4 intervein, while lower levels of Hh signalling direct L3 development (Crozatier et al., 2003). Therefore all patterning defects observed when *moe* expression is reduced, reduction in the L3/L4 intervein and expanded L3 vein, are indicative to alterations in Hh signalling. Interestingly, circles and thickening of the L3 vein very similar to those of moe^{c858} wings are observed when the function of the Hh receptor Ptc is reduced in mitotic recombination clones (Phillips et al., 1990), or modified by the expression of dominant-negative Ptc proteins (Strutt et al., 2001). The similarity between the phenotype of *ptc* and moe^{c858} wings in the L3 suggest that Moe modifies Hh signalling. We want to point out that we did not find any morphological alterations in the wing consistent with failures in signalling through the Notch, EGFR, Wg and Dpp pathways, suggesting that the effects of *moe* mutants are specific to the Hh pathway. For this reason, we think that the alterations in Hh signalling detected in *moe* mutant discs are not a consequence of the epithelial defects characteristics of these discs, because if this were the case, we would expect much more pleiotropic phenotypes than the observed local effects in the Hh domain of signalling.

The expression of high-threshold Hh-target genes is reduced when *moe* expression is lowered. Contrariwise, the domains of expression of Hh-targets activated by low levels of signalling are moderately expanded. These changes can be correlated with the reduced size of the L3/L4 intervein (lowered high-threshold response) and the thickened L3 vein (expanded low-threshold responses). It is likely that the lower levels

of *ptc* expression contribute to the observed expansion of cell fates determined by low levels of Hh signalling, because reduced Ptc would favour Hh spreading towards more anterior cells. Complementary, the failure to observe this expansion in discs where Moe expression is specifically reduced in the domain of *ptc* expression (see supplementary Figure 2), suggest that Moe activity in the low-threshold domain directly contribute to its dimension.

Our analysis does not establish a molecular mechanism linking Moe to Hh signalling, but indicates that most aspects of this function depend on the regulation of RhoA activity. The molecular mechanisms underlying the function of the RhoA GTPase are not yet clear, and include regulation of the actin cytoskeleton and membrane trafficking in the cytoplasm (Magie and Parkhurst, 2005; Malbon, 2005). There are several aspects of Hh signalling where Moe/RhoA activity might be required in the anterior compartment. The first is the localisation of Ptc to particular membrane domains where it would be capable of capturing Hh. When Moe expression is reduced the efficiency of Ptc-Hh interaction would be diminished and, consequently, decreased Hh signalling would occur at sites where Hh is required to trigger activation of high-threshold targets. In support of this possibility, interactions between Moe and Ptc proteins have been detected in two-hybrids assays (PimRyder database, Hybrigenics SA at https://pim.hybrigenics.com/prv31/cdsviewer/flybase.jsp). However, we have failed to observed consistent co-localisation in the cell membrane of Ptc and Moe. A second alternative is that Moe/RhoA are required for the internalization of Smo from the cell membrane and/or the intracellular sorting of Ptc/Hh and active Smo in the late endosome–lysosome system, which are critical for the regulation of the Hh signalling pathway (Incardona et al., 2002). In this case, a reduction in Moe would reduce Smo

activation, which would be more critical in cells requiring higher Smo activity. Interestingly ERM protein are involved in membrane trafficking, having a specialized function in the endocytic sorting of internalized 2-adrenergic receptor (Cao et al., 1999). Similarly, RhoA activity has a general role in signalling pathways involving membrane trafficking during early embryonic development (Magie and Parkhurst, 2005). Finally, it is also possible that Moe is required for different aspect of Hh signalling in the low and high-activity domains. Indeed it has been proposed that the high- and low-threshold responses to Hh are determined by different modes of Hh signalling involving specific components of the pathway (Hooper, 2003). In this scenario, RhoA may be directly stimulating Hh signalling in the low-threshold domain, as it seems to be the case of the human RhoA homolog, which is involved in mediating the response to Sonic hedgehog in vertebrate cells (Kasai et al., 2004). Further biochemical analysis will be necessary to determine the exact role of Moe in Hh signalling and its relationships with RhoA activity.

In conclusion, we find that *moe* has functions related to morphogenesis, cell shape, cell survival and epithelial organisation in the wing blade and hinge region. These requirements add to the known function of Moe in the maintenance of epithelial integrity in the wing blade. In addition, a novel function of Moe regulates Hh signalling, at least in the *Drosophila* wing disc. The molecular mechanism by which Moe affects Hh signalling is unknown, but Moe function appears critical for both the generation of high-levels of Hh signalling and the regulation of low-threshold target gene expression.

4. Experimental Procedures

4.1. Genetic strains

We used the *moe* alleles moe^{PL106}, moe^{G0323}, moe^{X5} (Polesello et al., 2002) and moe^{C858} (this work), the rhoA alleles $rhoA^{P1}$ and $rhoA^{P2}$ (Strutt et al., 1997), and the strains $ptclacZ^{AT96}$ (Lawrence et al., 1999), ptc^{IN}, tkv^{a12}, dpp^{d12}, smo^{3}, *Gal4-638* and *Gal4-sal*. Strains not described in the text can be found in flybase (Drysdale et al., 2005). *UAS-moe RNAi* lines were kindly provided by Sue Karagiosis (Karagiosis and Ready, 2004). Fly strains were cultured at 25º C. Wings were mounted in lactic acid-ethanol (1:1) and photographed with a Spot digital camera and a Zeiss Axioplan microscope. Wing measures were taken using NIH Image software.

4.2. Immunocytochemistry

We used rabbit anti-phosphorylated Mad (Tanimoto et al., 2000), anti-Moe (McCartney and Fehon, 1996), anti-Dll (Vachon et al., 1992), anti-Kn (Crozatier et al., 2002), anti-LanA (Kumagai et al., 1997), anti-Scrib (Bilder and Perrimon, 2000), anti-Vg (Kim et al., 1996), anti-Sal (de Celis and Barrio, 2000), anti-Hth (Casares and Mann, 1998) and anti-activated Cas3 (Cell Signalling), mouse monoclonals anti-Bs (Affolter et al., 1994), anti-Nb (Ng et al., 1995) and anti-Ptc (Capdevila et al., 1994), and rat anti-Vvl (Llimargas and Casanova., 1997), anti-Caup (Gómez-Skarmeta and Modolell, 1996) and anti-Ci (Aza-Blanc et al., 1997). Mouse monoclonals anti-En, anti-Dlg, anti-Arm, anti-N^{intra}, anti-Ct, anti-Wg and anti-FasIII (Hybridoma bank). Secondary antibodies were from Jackson Immunological Laboratories (used at 1/200 dilution). Imaginal wing discs were dissected, fixed and stained as described in (de Celis, 1997). Confocal images were captured with a BioRad confocal microscope, using the same setting for

mutant and control discs. We generated stacks of between 80 and 100 sections for each imaginal disc, with the distance between consecutive planes set at 0.45μm. Z-sections were generated from these stacks using Metaview software. In situ hybridization with *dpp* and *moe* RNA probes were carried out as described in de Celis (1997). We used the EST *RE10905* as a template to synthesise the *moe* probe.

4.3. Molecular mapping of moe alleles

moe^{C858} was mapped by inverse PCR following the protocol described in Berkeley (http://www.fruitfly.org/about/methods/index.html). Fine mapping of moe^{PL106}, moe^{G0323}, moe^{X5} and moe^{C858} was done by sequencing PCR products obtained using as a template genomic DNA from heterozygous flies. For the moe^{C858} allele we made a PCR with the oligonucleotides TTACCCAGGCGGTCAGTGTCG and CGACGGGACCACCTTATGTTA and another PCR with the oligonucleotides GCCCATCTCTTGAAGGACTCT and CGACGGGACCACCTTATGTTA. For mapping the insertions of moe^{PL106}, moe^{G0323} and moe^{X5} we made a PCR with the oligonucleotides TTACCCAGGCGGTCAGTGTCG and CACCCAAGGCTCTGCTCCCACAAT and another PCR with the oligonucleotides GCCCATCTCTTGAAGGACTCT and CAATCATATCGCTGTCTCACTCA. The resulting PCR products were cloned in pGEM-T-Easy (Promega) and sequenced using the oligonucleotides SP6 and T7. The resulting sequences were aligned with the *moe* genomic sequence.

Acknowledgements

We are very grateful to R. Hernandez and A. López-Varea for their skilful technical help. We also thank A. García-Bellido for his continuous support, D. Gubb, L. A. Baena, A. Baonza, R. Barrio, S. Campuzano, A. Glavic and S. Sotillos for critical reading of the manuscript. We also thank the Hybridome bank at Iowa University and many researchers for providing the tools necessary for this work. Grants from Dirección General de Investigación Científica y Técnica (BCM2003-1191 and GEN2001-4846-C05-01) to J.F.d C. and an institutional grant from Fundación Ramón Areces to the Centro de Biología Molecular "Severo Ochoa" are also acknowledged.

References

Affolter M., Montagne J., Walldorf U., Groppe J., Kloter U., LaRosa M., Gehring W. J. 1994. The Drosophila SRF homolog is expressed in a subset of tracheal cells and maps within a genomic region required for tracheal development. Development 120,743-53.

Apionishev S., Katanayeva N. M., Marks S. A., Kalderon D., Tomlinson A. 2005. Drosophila Smoothened phosphorylation sites essential for Hedgehog signal transduction. Nat Cell Biol 7, 86-92.

Aza-Blanc P., Ramirez-Weber F. A., Laget M. P., Schwartz C., Kornberg T. B. 1997. Proteolysis that is inhibited by hedgehog targets Cubitus interruptus protein to the nucleus and converts it to a repressor. Cell 89, 1043-53.

Barreiro O., Yanez-Mo M., Serrador J. M., Montoya M. C., Vicente-Manzanares M., Tejedor R., Furthmayr H., Sanchez-Madrid F. 2002. Dynamic interaction of VCAM-1 and ICAM-1 with moesin and ezrin in a novel endothelial docking structure for adherent leukocytes. J Cell Biol 157, 1233-45.

Baumgartner M., Patel H., Barber D. L. 2004. Na+/H+ exchanger NHE1 as plasma membrane scaffold in the assembly of signaling complexes. Am J Physiol Cell Physiol 287, 844-50.

Bijlsma M. F., Spek C. A., Peppelenbosch M. P. 2004. Hedgehog: an unusual signal transducer. Bioessays 26, 387-94.

Bilder B., Perrimon N. 2000. Localization of apical epithelial determinants by the basolateral PDZ protein Scribble. Nature 403, 676-80.

Bretscher A. 1999. Regulation of cortical structure by the ezrin-radixin-moesin protein family. Curr Opin Cell Biol 11, 109-16.

Bretscher A., Chambers D., Nguyen R., Reczek D. 2000. ERM-Merlin and EBP50 protein families in plasma membrane organization and function. Annu Rev Cell Dev Biol 16, 113-43.

Bretscher A., Edwards K., Fehon, R. G. 2002 ERM proteins and merlin: integrators at the cell cortex. Nat Rev Mol Cell Biol 3, 586-99.

Bretscher A., Reczek D., Berryman M. 1997. Ezrin: a protein requiring conformational activation to link microfilaments to the plasma membrane in the assembly of cell surface structures. J Cell Sci 110, 3011-8.

Cao T. T., Deacon H. W., Reczek D., Bretscher A., von Zastrow M. 1999. A kinase-regulated PDZ-domain interaction controls endocytic sorting of the beta2-adrenergic receptor. Nature 401, 286-90.

Capdevila J., Pariente F., Sampedro J., Alonso J. L., Guerrero I. 1994. Subcellular localization of the segment polarity protein patched suggests an interaction with the wingless reception complex in Drosophila embryos. Development 120, 987-98.

Casares F., Mann R. S. 1998. Control of antennal versus leg development in *Drosophila*. Nature 392, 723-6.

Chen Y., Struhl G. 1996. Dual roles for Patched in sequestering and transducing Hedgehog. Cell 87, 553-563.

Crozatier M., Glise B., Khemici V., Vincent A. 2003. Vein-positioning in the Drosophila wing in response to Hh; new roles of Notch signaling. Mech Dev 120, 529-35.

Crozatier M., Glise B., Vincent A. 2002. Connecting Hh, Dpp and EGF signalling in patterning of the *Drosophila* wing; the pivotal role of *collier/knot* in the AP organiser. Development 129, 4261-4269.

de Celis J. F. 1997. Expression and function of decapentaplegic and thick veins in the differentiation of the veins in the *Drosophila* wing. Development 124, 1007-1018

de Celis J. F. 2003. Pattern formation in the Drosophila wing: the development of the veins. BioEssays 25, 443-451.

de Celis J. F., Barrio R. 2000. Function of the *spalt/spalt-related* gene complex in positioning the veins in the *Drosophila* wing. Mech Dev 91, 31-41.

Denef N., Neubuser, D., Perez L., Cohen, S. M. 2000 Hedgehog induces opposite changes in turnover and subcellular localization of patched and smoothened. Cell 102, 521-31.

Drysdale R. A., Crosby M. A., Gelbart W., Campbell K., Emmert D., Matthews B., Russo S., Schroeder A., Smutniak F., Zhang P., Zhou, P., Zytkovicz M., Ashburner M., de Grey A., Foulger R., Millburn G., Sutherland D., Yamada C., Kaufman T., Matthews K., DeAngelo A., Cook R. K., Gilbert D., Goodman J., Grumbling G., Sheth H., Strelets V., Rubin G., Gibson M., Harris N., Lewis S., Misra S., Shu S. 2005. FlyBase: genes and gene models. Nucleic Acids Res 33, 390-5.

Fehon R. G., Johansen K., Rebay I., Artavanis-Tsakonas S. 1991. Complex cellular and subcellular regulation of Notch expression during embryonic and imaginal development of Drosophila: implications for Notch function. J Cell Biol, 657-669.

Gary R., Bretscher A. 1995. Ezrin self-association involves binding of an N-terminal domain to a normally masked C-terminal domain that includes the F-actin binding site. Mol Biol Cell 6, 1061-75.

Giraldez A. J., Cohen S. M. 2003. Wingless and Notch signaling provide cell survival cues and control cell proliferation during wing development. Development 130, 6533-6543.

Gómez-Skarmeta J. L., Modolell J. 1996. *araucan* and *caupolican* provide a link between compartment subdivisions and patterning of sensory organs and veins in the *Drosophila* wing. Genes & Dev. 10, 2935-2945.

Hamada K., Shimizu T., Matsui T., Tsukita S., Hakoshima T. 2000. Structural basis of the membrane-targeting and unmasking mechanisms of the radixin FERM domain. Embo J 19, 4449-62.

Hamada K., Shimizu T., Yonemura S., Tsukita S., Hakoshima T. 2003. Structural basis of adhesion-molecule recognition by ERM proteins revealed by the crystal structure of the radixin-ICAM-2 complex. Embo J 22, 502-14.

Hipfner D. R., Keller N., Cohen S. M. 2004. Slik Sterile-20 kinase regulates Moesin activity to promote epithelial integrity during tissue growth. Genes Dev 18, 2243-8.

Hiscox S., Jiang W. G. 1999. Ezrin regulates cell-cell and cell-matrix adhesion, a possible role with E-cadherin/beta-catenin. J Cell Sci 112, 3081-3090.

Hooper J. E. 2003. Smoothened translates Hedgehog levels into distinct responses. Development 130:3951-63.

Huang L., Wong T. Y., Lin R. C ., Furthmayr H. 1999. Replacement of threonine 558, a critical site of phosphorylation of moesin in vivo, with aspartate activates F-actin binding of moesin Regulation by conformational change. J Biol Chem 274, 12803-10.

Incardona, J. P., Gruenberg, J., Roelink, H. 2002. Sonic hedgehog induces the segregation of patched and smoothened in endosomes. Curr Biol 12, 983-995.

Ingraffea J., Reczek D., Bretscher A. 2002. Distinct cell type-specific expression of scaffolding proteins EBP50 and E3KARP: EBP50 is generally expressed with ezrin in specific epithelia, whereas E3KARP is not. Eur J Cell Biol 81, 61-8.

Ivetic A., Ridley A. J. 2004. Ezrin/radixin/moesin proteins and Rho GTPase signalling in leucocytes. Immunology 112, 165-76.

Jankovics F., Sinka R., Lukacsovich T., Erdelyi M. 2002. MOESIN crosslinks actin and cell membrane in *Drosophila* oocytes and is required for OSKAR anchoring. Curr Biol 12, 2060-5.

Jia J., Tong C., Wang B., Luo L., Jiang J. 2004. Hedgehog signalling activity of Smoothened requires phosphorylation by protein kinase A and casein kinase I. Nature 432, 1045-50.

Karagiosis S. A., Ready D. F. 2004. Moesin contributes an essential structural role in Drosophila photoreceptor morphogenesis. Development 131, 725-32.

Kasai, K., Takahashi, M., Osumi, N., Sinnarajah, S., Takeo, T., Ikeda, H., Kehrl, J. H., Itoh, G. and Arnheiter, H. 2004. The G12 family of heterotrimeric G proteins and Rho GTPase mediate Sonic hedgehog signalling. Genes Cells 9, 49-58.

Kim J., Sebring A., Esch J. J., Kraus M. E., Vorwerk K., Magee J., Carroll S. B. 1996. Integration of positional signals and regulation of wing formation by Drosophila vestigial gene. Nature 382, 133-138.

Klein T., Martinez Arias A. 1988. Different spatial and temporal interactions between Notch, wingless, and vestigial specify proximal and distal pattern elements of the wing in Drosophila. Dev Biol 194, 196-212

Kumagai C., Kadowaki T., Kitagawa Y. 1997. Disulfide-bonding between *Drosophila* laminin beta and gamma chains is essential for alpha chain to form alpha betagamma trimer. FEBS Lett 412, 211-6.

Lawrence, P. A., Casal, J., Struhl, G. 1999. hedgehog and engrailed: pattern formation and polarity in the Drosophila abdomen. Development 126, 2431-2439.

Llimargas M., Casanova J. 1997. ventral veinless, a POU domain transcription factor, regulates different transduction pathways required for tracheal branching in *Drosophila*. Development 124, 3273-3281.

Louvet-Vallee S. 2000. ERM proteins: from cellular architecture to cell signaling. Biol Cell 92, 305-16.

Lum L., Beachy P. A. 2004. The Hedgehog response network: sensors, switches, and routers. Science 304, 1755-9.

Malbon, C.C. 2005. G Proteins in development. Nature reviews Mol Cell Biol. 6, 689-701.

Martin V., Carrillo G., Torroja C., Guerrero I. 2001. The sterol-sensing domain of Patched protein seems to control Smoothened activity through Patched vesicular trafficking. Curr Biol 11, 601-7.

McCartney B .M., Fehon R. G. 1996. Distinct cellular and subcellular patterns of expression imply distinct functions for the *Drosophila* homologues of moesin and the neurofibromatosis 2 tumor suppressor, merlin. J Cell Biol 133, 843-52.

Mullor J. L., Calleja M., Capdevila J., Guerrero I. 1997. Hedgehog activity, independent of Decapentaplegic, participates in wing disc patterning. Development 124, 1227-1237.

Nakano Y., Nystedt S., Shivdasani A. A., Strutt H., Thomas C., Ingham P. W. 2004. Functional domains and sub-cellular distribution of the Hedgehog transducing protein Smoothened in *Drosophila*. Mech Dev 121, 507-18.

Ng M., Diaz-Benjumea F. J., Cohen S. M. 1995. Nubbin encodes a POU-domain protein required for proximal-distal patterning in the *Drosophila* wing. Development 121, 589-99.

Oshiro N., Fukata Y., Kaibuchi K. 1998. Phosphorylation of moesin by rho-associated kinase Rho-kinase plays a crucial role in the formation of microvilli-like structures. J Biol Chem 273, 34663-6.

Pearson M. A., Reczek D., Bretscher A., Karplus P. A. 2000. Structure of the ERM protein moesin reveals the FERM domain fold masked by an extended actin binding tail domain. Cell 101, 259-70.

Perez-Garijo, A., Martin, F. A. and Morata, G. (2004). Caspase inhibition during apoptosis causes abnormal signalling and developmental aberrations in Drosophila. Development 131, 5591-8.

Perez-Garijo, A., Martin, F. A., Struhl, G. and Morata, G. 2005. Dpp signaling and the induction of neoplastic tumors by caspase-inhibited apoptotic cells in *Drosophila*. Proc Natl Acad Sci U S A 102, 17664-17669.

Phillips R. G., Roberts I. J., Ingham P. W., Whittle J.R.S. 1990. The Drosophila segment polarity gene patched is involved in a position-signalling mechanism in imaginal discs Development 110, 105-114.

Polesello C., Delon I., Valenti P., Ferrer P., Payre F. 2002. *Dmoe* controls actin-based cell shape and polarity during *Drosophila melanogaster* oogenesis. Nat Cell Biol 4, 782-9.

Polesello C., Payre F. 2004. Small is beautiful: what flies tell us about ERM protein function in development. Trends Cell Biol 14, 294-302.

Reczek D., Berryman M., Bretscher A. 1997. Identification of EBP50: A PDZ-containing phosphoprotein that associates with members of the ezrin-radixin-moesin family. J Cell Biol 139, 169-79.

Rodriguez del Alamo, D., A., Terriente, J., Galindo, M. I., Couso, J. P. and Diaz-Benjumea, F. J. (2002). Different mechanisms initiate and maintain wingless expression in the Drosophila wing hinge. Development 129, 3995-4004.

Speck O., Hughes S. C., Noren N. K., Kulikauskas R. M., Fehon R. G. 2003. Moesin functions antagonistically to the Rho pathway to maintain epithelial integrity. Nature 421, 83-7.

Strutt, D. I., Weber, U. and Mlodzik, M. 1997. The role of RhoA in tissue polarity and Frizzled signalling. Nature 387, 292-295.

Strutt H., Thomas C., Nakano Y., Stark D., Neave B., Taylor A. M., Ingham P. W. 2001. Mutations in the sterol-sensing domain of Patched suggest a role for vesicular trafficking in Smoothened regulation. Curr Biol 11, 608-13.

Takeuchi K., Kawashima A., Nagafuchi A., Tsukita S. 1994. Structural diversity of band 4.1 superfamily members. J Cell Sci 107, 1921-1928.

Tanimoto H., Itoh S., ten Dijke P., Tabata T. 2000. Hedgehog creates a gradient of DPP activity in Drosophila wing imaginal discs. Molecular Cell 5, 59-71.

Toba G., Ohsako T., Miyata N., Ohtsuka T., Seong K. H., Aigaki T. 1999. The gene search system: a method for efficient detection and rapid molecular identification of genes in *Drosophila melanogaster*. Genetics 151, 725-737.

Torroja C., Gorfinkiel N., Guerrero I. 2004. Patched controls the Hedgehog gradient by endocytosis in a dynamin-dependent manner, but this internalization does not play a major role in signal transduction. Development 131, 2395-408.

Tsukita S., Yonemura S. 1999. Cortical actin organization: lessons from ERM ezrin/radixin/moesin proteins. J Biol Chem 274, 34507-10.

Vachon G., Cohen B., Pfeifle C., McGuffin M. E., Botas J., Cohen S. M. 1992. Homeotic genes of the *Bithorax* complex repress limb development in the abdomen of the *Drosophila* embryo through the target gene Distal-less. Cell 71, 437-50.

van den Heuvel M. 2003. Hedgehog signalling: off the shelf modulation Curr Biol 13, 686-8.

Yonemura S., Matsui T., Tsukita S. 2002. Rho-dependent and -independent activation mechanisms of ezrin/radixin/moesin proteins: an essential role for polyphosphoinositides in vivo. J Cell Sci 115, 2569-80.

Yonemura S., Tsukita S. 1999. Direct involvement of ezrin/radixin/moesin ERM-binding membrane proteins in the organization of microvilli in collaboration with activated ERM proteins. J Cell Biol 145, 1497-509.

Zhang W., Zhao Y., Tong C., Wang G., Wang B., Jia J., Jiang J. 2005. Hedgehog-regulated costal2-kinase complexes control phosphorylation and proteolytic processing of cubitus interruptus. Dev Cell. 8, 267-78.

Zhu A. J., Zheng L., Suyama K., Scott M. P. 2003. Altered localization of *Drosophila* Smoothened protein activates Hedgehog signal transduction. Genes Dev 17, 1240-52.

LEGENDS TO FIGURES

Table 1

Frequencies of phenotypic classes in *moe*^{c858} males and *moe* heteroallelic combinations. Red, yellow and blue bars indicate the frequency of strong (Red), intermediate (orange) and weak (blue) phenotypes of wing vesicles (A) and L3 defects (B). The first column (C858) corresponds to *moe*^{c858} hemizygous males, the next two columns correspond to *moe*^{c858}/*moe*^{PL106} (C858/PL106) and *moe*^{c858}/*moe*^{G0323} (C858/G0323) females. The C858; rhoA/+ column corresponds to *moe*^{c858} males heterozygous for the *rhoA* mutation *rhoA*^{P1}. The last column to the right (C858; salGal4) corresponds to *moe*^{c858}; *sal-Gal4*/+ males. In this genotype the expression of *moe* is induced in the *sal* domain of expression (between the veins L2 and L5).

Figure 1

Adult phenotype of loss of *moe* function.

(A) Wild type wing showing the positions of the veins L2 to L5. (B-C) Mutant *moe*^{c858} wings corresponding to the weak (B) and strong (C) phenotypic classes. (D-E) Reduced wing size, wing vesicles (arrows) and L3 defects (arrowheads) in adult wings of the combinations *moe*^{c858}/*moe*^{PL106} (D) and *moe*^{c858}/*moe*^{G0323} (E). (F) Adult wing of the combination *638-Gal4*/*UAS-moeRNAi*, with a phenotype similar to the *moe*^{c858} wings shown in (C). (G-H) Higher magnification of the hinge region in a wild type wing (G) and in a *moe*^{c858} wing (H), showing the pattern disorganisation of the wing base. (I) Wing-hinge vesicles trapped between the dorsal and ventral wing surfaces in *moe*^{c858} flies. Successive focal planes of the same wing showing the localisation of a wing tissue vesicle: dorsal (J), vesicle (J') and ventral (J''). (K-M) Common alterations in the L3

vein (wild type L3 is shown in K) in *moe*^{c858} wings, varying from circles of L3 vein (L) to severe thickening of L3 (M).

Figure 2

Numerical parameters of wild type and *moe* mutant wings.

(A) Measures of wing size and cell number in wild type (yellow rows) and *moe*^{c858}/*moe*^{G0323} adult wings (blue rows).

Distance L3/L4: number of cells in width between the veins L3 and L4 in the position of the posterior crossvein (red line in B).

Area: Number of cells in a square positioned in the L3/L4 intervein (black square in C).

Wing: Number of wing cells (yellow shadow in B).

L3-L4: Number of cells in the L3/L4 intervein (red shadow in C).

L2-L3: Number of cells in the L2/L3 intervein (green shadow in C).

L5: Number of cells in the L5/Posterior wing margin region (blue shadow in C).

Ratio: Proportion of different wing territories in wild type and mutant wings relative to wing size or to the size of other wing territories.

Signification: Significance of the difference between wild type and mutant wings using the T-Student algorithm.

Length: Number of pixels between the hinge and the distal wing margin in the position of L3 vein (black horizontal line in B).

Width: Number of pixels between the anterior and posterior wing margin (black vertical line in B).

(B-C) Schematic representation of the wing showing the territories used in the different measures shown in (A). (B) Wing territory measured in 10 wild type and 20 *moe*^{c858}/*moe*^{G0323} adult wings (yellow shadow). (C) L2/L3 intervein territory measured in

10 wild type and 20 moe^{c858}/moe^{G0323} adult wings (green shadow), L3-L4 intervein territory measured in 10 wild type and 20 moe^{c858}/moe^{G0323} adult wings (red shadow), L5-posterior wing margin territory measured in 10 wild type and 20 moe^{c858}/moe^{G0323} adult wings (blue shadow) and area used to measure cell density (black square). The number of cells between the veins L3 and L4 was measured in the region showed by a red line in B. The length and width of the wings was measured in the region showed by black lines in B. We only considered the *moe* wings with the weakest phenotype (see Fig. 1B).

Figure 3

Map of the *moe* gene and localisation of the P insertions. Expression of *moe* RNA and protein in moe^{c858} wing discs.

(A) Schematic representation of the *moe* coding region (modified from *flybase*) showing the coding (red boxes) and non-coding exons (blue boxes), the alternative ATG of different transcripts and the localisation of the *moe* alleles (yellow triangle) used in this study. (B) Nucleotide sequence of exon 1b, with the exact localisation of the insertion sites (small coloured triangles) of the alleles moe^{X5}, moe^{G0323}, moe^{PL106} and moe^{c858}. (C-E) Expression of *moe* mRNA in wild type (C), moe^{c858} (D) and moe^{PL106} (E) wing discs. In situ hybridisations were carried out with the same probe concentration and developed for the same period of time. (F-G) Expression of Moe protein in wild type (F) and moe^{c858} discs (G). Tangential sections along the proximal-distal and anterior-posterior axes of the discs are shown at the right side and below, respectively, of the corresponding discs. Two longitudinal sections, label 1 and 2 along the wing blade (1) and hinge (2) of the moe^{c858} disc are shown in G. Cells located below the epithelium show increased levels of Moe expression (white arrow in section 2).

Figure 4

Expression of the epithelial markers Armadillo (Arm) and LamininA (LanA) in wild type and *moe*^{c858} mutant wing discs.

In all panels, each tangential section is accompanied by its corresponding Z-sections along the proximo-distal and antero-posterior axes. In all pictures Arm expression is in green and LanA in red, except in D where Cas3 expression is in red. White lines indicate the position of the Z-sections. (A) Sub-apical section of a mature wild type wing disc, showing in Z-sections the squamous peripodial layer (white arrow) and the columnar wing epithelium (white arrowhead) connected by a characteristic pattern of folds. Schematic drawing of the proximo-distal Z-section is shown to the right, indicating the basal lamina (red) and the apical side (green) of the epidermal cells. The apical side of the epithelium is oriented to the left. (B-C) Expression of Arm (green) and LanA (red) in *moe*^{c858} wing discs in an apical (B) and basal (C) transversal sections. Note that the apical expression of Arm in the wing blade is not affected, whereas the expression of LanA is severely affected, particularly in the regions corresponding to the folds (white arrows in C). (D) Expression of Arm (green) and activated Caspase 3 (Cas3 in red) in a *moe*^{c858} wing disc. The cells expressing Cas3 are shadowed in red in the schematic draw show to the right. (E-F) *638-Gal4/UAS-moeRNAi* discs in a sub-apical section through the wing blade (E) and in a basal section through the wing hinge (F). The expression of Arm is still localised to the apical side of the cells in the wing blade (E). The expression of both Arm and LanA is very disrupted in the hinge region, where the epithelium losses its continuity (F).

(G-I) Schematic representations of anterior-posterior Z-sections along the wing blade in wild type (G) and both *638-Gal4/UAS-moeRNAi* and *moe*^{c858}, which are identical, in the

wing blade (H), and along the wing hinge (I). The apical side is in green; the basal lamina in red and the nuclei are represented as black dots. Breaking of the basal lamina is represented by a dotted line.

Figure 5

Expression of the epithelial markers Armadillo (Arm) and LamininA (LanA) in wild type and *moe*^{PL106} mutant wing discs.

(A-C) Expression of Armadillo (Arm in green) and LamininA (LanA in red) in wild type (A) and *moe*^{PL106} early third instar discs (B-C). Note the abnormal accumulation of Arm in *moe*^{PL106} early discs (B), and the abnormal structure of the basal lamina (C). (D) Schematic representations of proximo-distal Z-sections in a wild type (left) and *moe*^{PL106} wing discs along the wing blade. The apical side is in green; the basal lamina in red and the nuclei are represented as black dots. Breaking of the basal lamina is represented by a dotted line. (E-G) Expression of Arm (green) in a late third instar *moe*^{PL106} wing disc in three different focal planes (white line on the cross section) showing the normal apical localisation of Arm (E and G), the abnormal folding of the disc (G) and the formation of vesicles (arrowhead in F). (H) Schematic representations of the proximo-distal Z-sections in *moe*^{PL106} along the wing blade. The apical side is in green; the inferred position of the basal lamina is in black, as it was not directly labelled in this experiment, and the nuclei are represented as black dots.

Figure 6

Cell fates in wild type and *moe*^{c858} mutant wing discs using nuclear markers.

(A-E) Expression of cell-fate markers in wild type discs labelling the wing blade (Vg, green in A), the central region of the wing (Sal, green in B), the hinge (Hth, green in C),

the wing blade and hinge (Nub, green in D), and the posterior compartment (En, green in E) of wild type wing discs. The expression of Wg is shown in B (red). The expression of LanA (red in D and E), Arm (red in C) and FasIII (red in A) delimits the morphology of the epithelium.

(F-J) Expression of the same cell-fate markers in *moe*^{c858} wing discs: Vg (green in F), Sal (green in G), Hth (green in H), Nub (green in I) and En (green in J). The expression of Wg is shown in G (red) and the expression of LanA (red in I and J), Arm (red in H) and FasIII (red in F) delimits the morphology of the epithelium. (J') Schematic drawing of En expression in an anterior-posterior section of a *moe*^{c858} disc. (K-T) Schematic representation of cell fate markers in transversal sections along the proximal-distal wing disc in wild type (WT) and mutant *moe*^{c858} (moe) discs. The region of expression for each marker is draw in red.

Figure 7

Expression of Notch, Dpp and Wingless targets in wild type and *moe*^{c858} discs.

(A-D) Expression in wild type discs of Distalless (Dll in A), Ventral veinless (Vvl in B), Cut (Ct in C) and Phosphorylated Mad (PMad in D). (E-H) Expression in *moe*^{c858} discs of Distalless (E), Ventral veinless (F), Cut (G) and Phosphorylated Mad (H). The white lines in D and H delimit the extent of the wing blade in wild type (D) and *moe*^{c858} discs, respectively. The expansion in width of P-Mad expression in the wing blade of *moe*^{c858} discs compared to wild type most likely is due to the broader expression of *dpp* characteristic of *moe*^{c858} mutant discs.

Figure 8

Expression of Hh-targets in wild type and in *moe* loss-of-function alleles.

(A-D) Expression of Ptc protein in wild type (A), *moe*^{c858} (B) and *moe*^{PL106} (C). Note the reduction in the level and wideness of the Ptc domain of expression. (D-D') Expression of nuclear lacZ (green) in *ptc-lacZ*/+ (D) and *moe*^{c858}*; ptc-lacZ*/+ males (D'). The expression of *ptc* is reduced in the mutant compared to the wild type discs. (E-F) Expression of Ci (Ci; green in E) and Knot (Kn; red in E) in a wild type disc. Separate channels are shown in F for Ci, and as an inset for Kn. (G-H) Expression of Caup (caup; green) and Knot (Kn; red) in a wild type disc. The expression of Caup is also shown in H. (I-J) Expression of Ci (Ci; green) and Kn (Kn; red) in a *moe*^{c858} wing disc. Separate channels are shown in J. (K-L) Expression of Caup (Caup; green) and Knot (Kn; red) in a *moe*^{c858} wing disc. The expression of Caup is also shown in L. The L3 vein is indicated by an arrow. (M-N) Expression of En in wild type (M) and *moe*^{c858} (N) discs. The anterior-posterior compartment boundary is indicated by a white arrow in M and N and the extent of the anterior expression of En by a white line in M. (O-P) Expression of *dpp* mRNA in wild type (O) and *moe*^{c858} (P) discs.

Figure 9

(A-B) Expression of Ptc (green) and Moe (red) in wild type discs. Longitudinal Z-sections are shown in B. The accumulation of Moe occurs in the apical side of both the peripodial and wing blade epithelia. (C-D) Expression of Ptc (green) and Moe (Red) in *moe*^{c858} discs. Longitudinal Z-sections are shown in D. (E) Expression of Ptc (green) and Moe (red) in a group of cells located underneath the wing blade epithelium in *moe*^{c858} discs. (F-G) Summary of Hh-target expression in Wild type (left) and *moe*^{c858} (right). The vertical black line represents the A/P compartment boundary, the size and height of each coloured box represents the extent and level of expression, respectively, of the corresponding gene. (H) Frequency of strong (red), moderate (orange) and weak

(blue) L3 defects in *moe*^{c858} males heterozygous for strong alleles of *ptc* (*ptc*^{IN}), *smo* (*smo*^{3}), *thick veins* (*tkv*^{a12}) and *dpp* (*dpp*^{d12}). Only the heterozygosis of *smo* (middle column) increases the phenotype of *moe*^{c858} flies.

Supplementary Figure 1

Expression of Patched (Ptc in green) and activated Caspase 3 (Cas in red) in wild type and *moe* mutant wing imaginal discs.

(A) Wild type discs showing the expression of ptc (green). (B-C) Expression of Ptc (green) and Cas3 (red) in two *moe*^{PL106}*; rhoA*^{P1}/+ wing imaginal discs (PL106; rho). B and C correspond to apical planes and B' and C' correspond to basal planes. (D-E) Expression of Ptc (green) and Cas3 (red) in two *moe*^{PL106} wing imaginal discs (PL106). D and E correspond to apical planes and D' and E' correspond to basal planes. Note the rescue of both Ptc expression (compare B and C with D and E) and cell death (compare B' and C' with D' and E'). (F-F') Expression of Ptc (green) and Cas3 (red) in *moe*^{c858}*; rhoA*^{P1}/+ wing imaginal disc (C858; rho). F and F' correspond to apical and basal planes, respectively. (G-G') Expression of Ptc (green) and Cas3 (red) in a *moe*^{c858} wing imaginal disc (C858). G and G' correspond to apical and basal planes, respectively.

Supplementary Figure 2

Effects of Moe reduction in the *ptc* domain of expression.

(A) Wild type wing. (B) *ptc-Gal4/UAS-moeRNAi* wing. Note the reduced wing size, the abnormal proximity between the veins L3 and L4, and the normal differentiation of the L3 vein (L3). (C) Expression of GFP (green) in a *ptc-Gal4/UAS-GFP* disc (Ptc, green). (D) Expression of Ptc in a wild type disc (Ptc, green). (E) Expression of Ptc in a

ptc-Gal4/UAS-moeRNAi discs (Ptc, green). (F-F'') Expression of FasIII (green) and activated Cas3 (Red) in a *ptc-Gal4/UAS-moeRNAi* discs in apical (F), medium-lateral (F') and tangential (F'') sections. (G-G') Expression of Ci (Ci, G) and Knot (Kn, G') in a wild type disc. (H-H') Expression of Ci (Ci, H) and Knot (Kn, H') in a *ptc-Gal4/UAS-moeRNAi* wing disc.

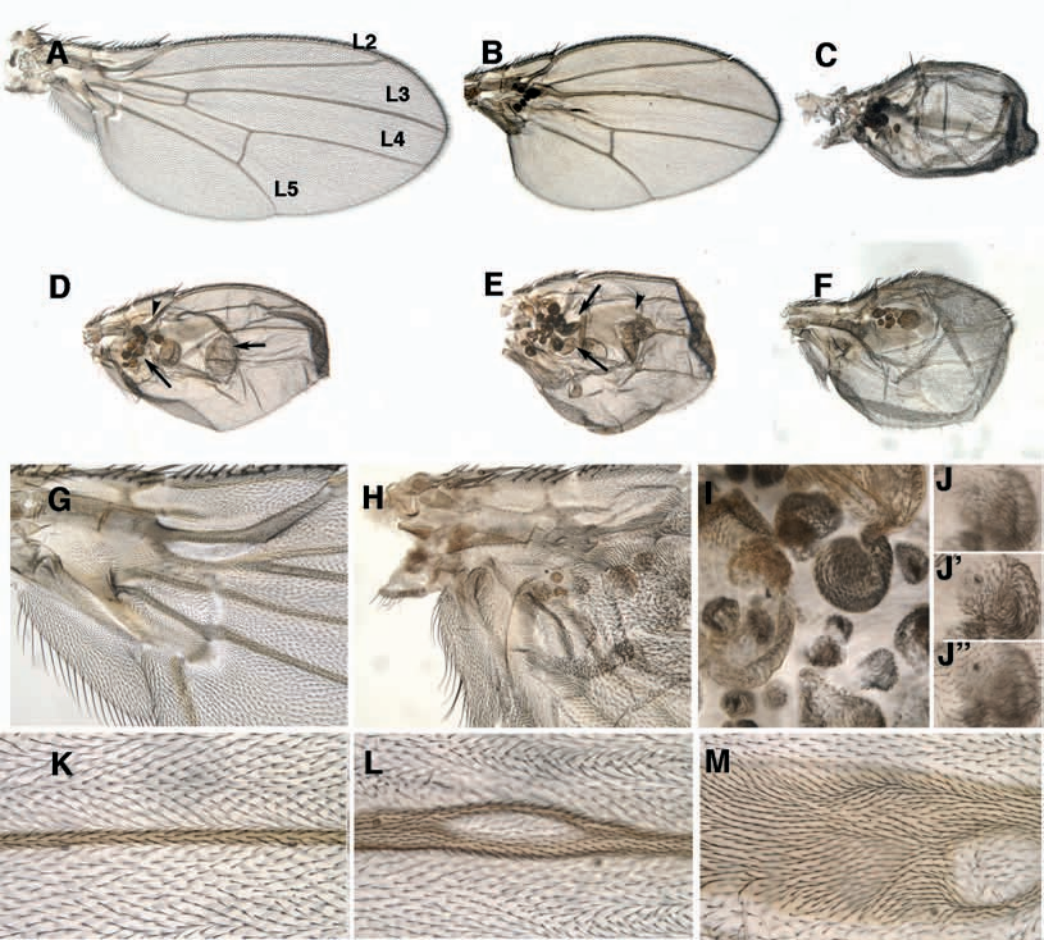
A
L2
L3
L4
L5
B
C
D
E
F
G
H
I
J
J'
J''
K
L
M

A

	Number of Cells					
	Distance L3-L4	Area	Wing	L3-L4	L2-L3	L5
M	17,68	152,7	10411,75	2100,06	1758,23	2336,16
SD	1,00	8,59	685,10	128,36	131,23	129,34
M	15,44	214,85	9295,09	1637,56	1670,08	2109,32
SD	1,97	23,70	1130,59	202,77	179,98	318,18
p	0,00000	0,00000	0,00239			

	Ratio					Pixels	
	L3-L4/Wing	L3-L4/L2-L3	L3-L4/L5	L2-L3/Wing	L5/Wing	Length	Width
M	0,20	1,20	0,90	0,17	0,22	571,44	291,74
SD	0,01	1,05	0,06	0,00	0,01	20,10	8,03
M	0,18	0,98	0,78	0,18	0,23	418,66	236,96
SD	0,01	0,09	0,06	0,01	0,02	28,85	12,38
p	0,00000	0,00000	0,00001	0,00208	0,73777	0,00000	0,00000

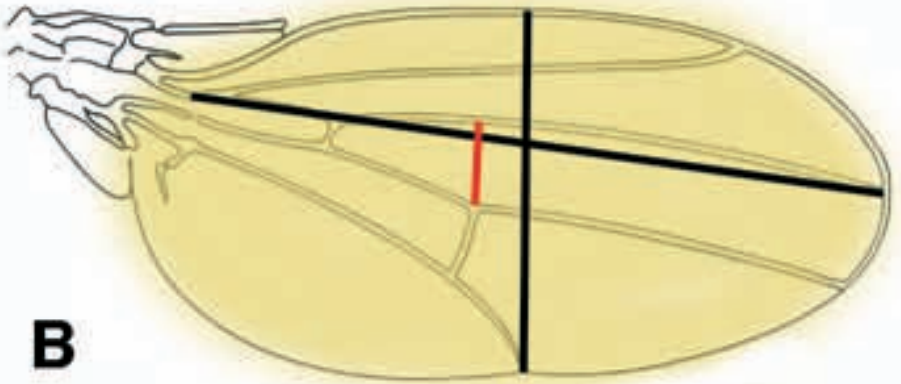

B

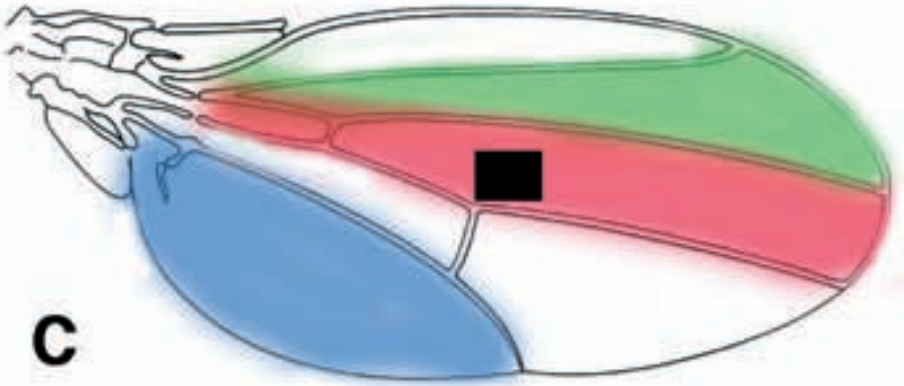

C

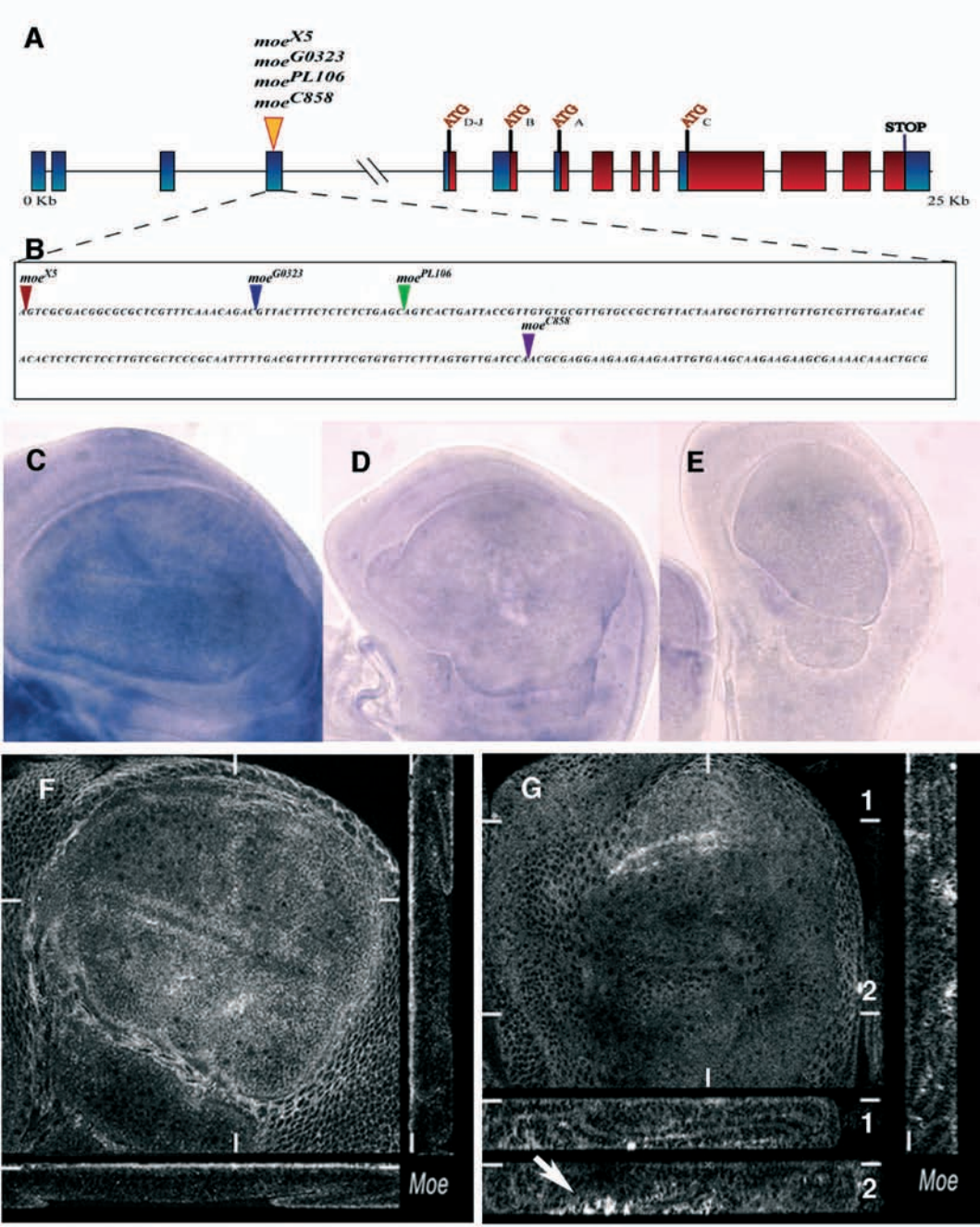
A
moeX5
moeG0323
moePL106
moeC858
ATG
D-J
ATG
B
ATG
A
ATG
C
STOP
0 Kb
25 Kb
B
moeX5
moeG0323
moePL106
moeC858
AGTCGCGACGGCGCGCTCGTTTCAAACAGACGTTACTTTCTCTCTCTGAGCAGTCACTGATTACCGTTGTGTGCGTTGTGCCGCTGTTACTAATGCTGTTGTTGTTGTCGTTGTGATACAC
ACACTCTCTCTCCTTGTCGCTCCCGCAATTTTTGACGTTTTTTTTCGTGTGTTCTTTAGTGTTGATCCAACGCGAGGAAGAAGAAGAATTGTGAAGCAAGAAGAAGCGAAAACAAACTGCG
C
D
E
F
Moe
G
1
2
1
2
Moe

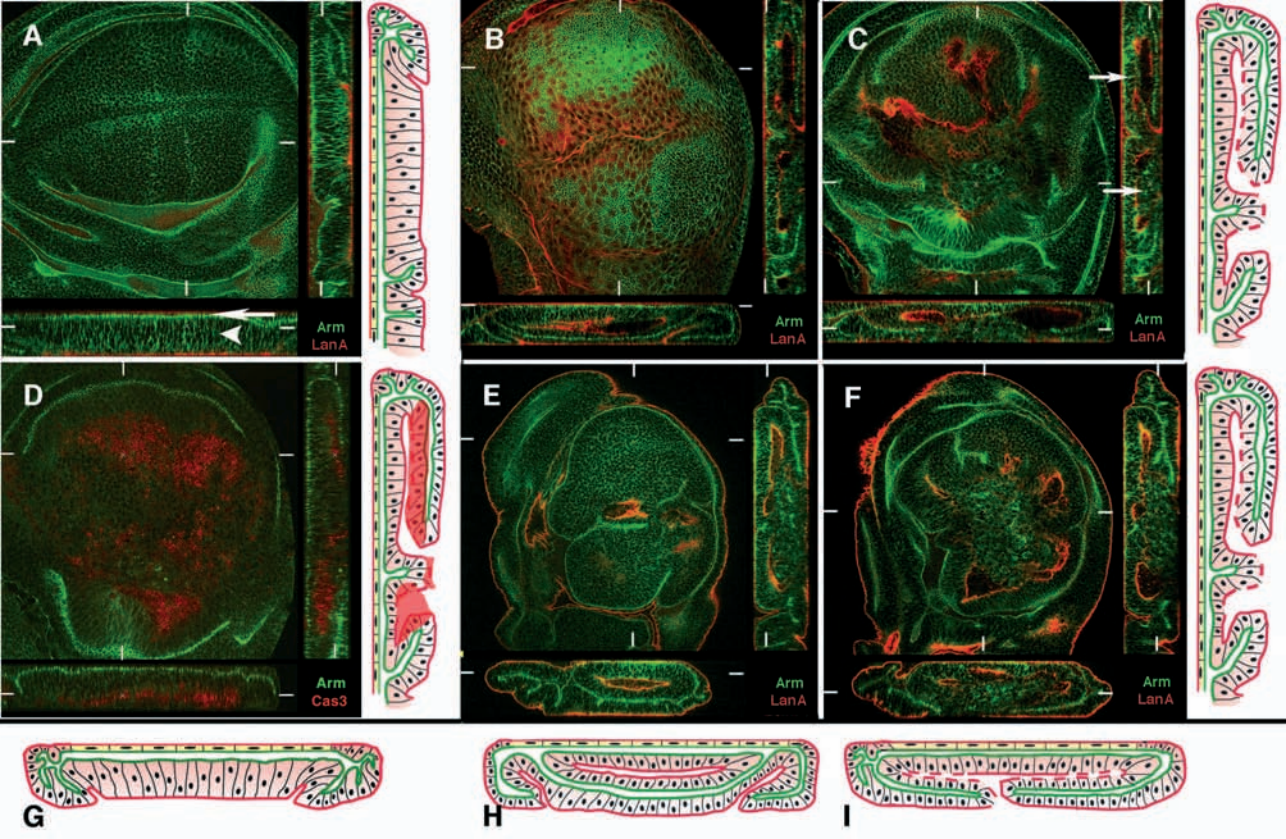
A
Arm
LanA
B
Arm
LanA
C
Arm
LanA
D
Arm
Cas3
E
Arm
LanA
F
Arm
LanA
G
H
I

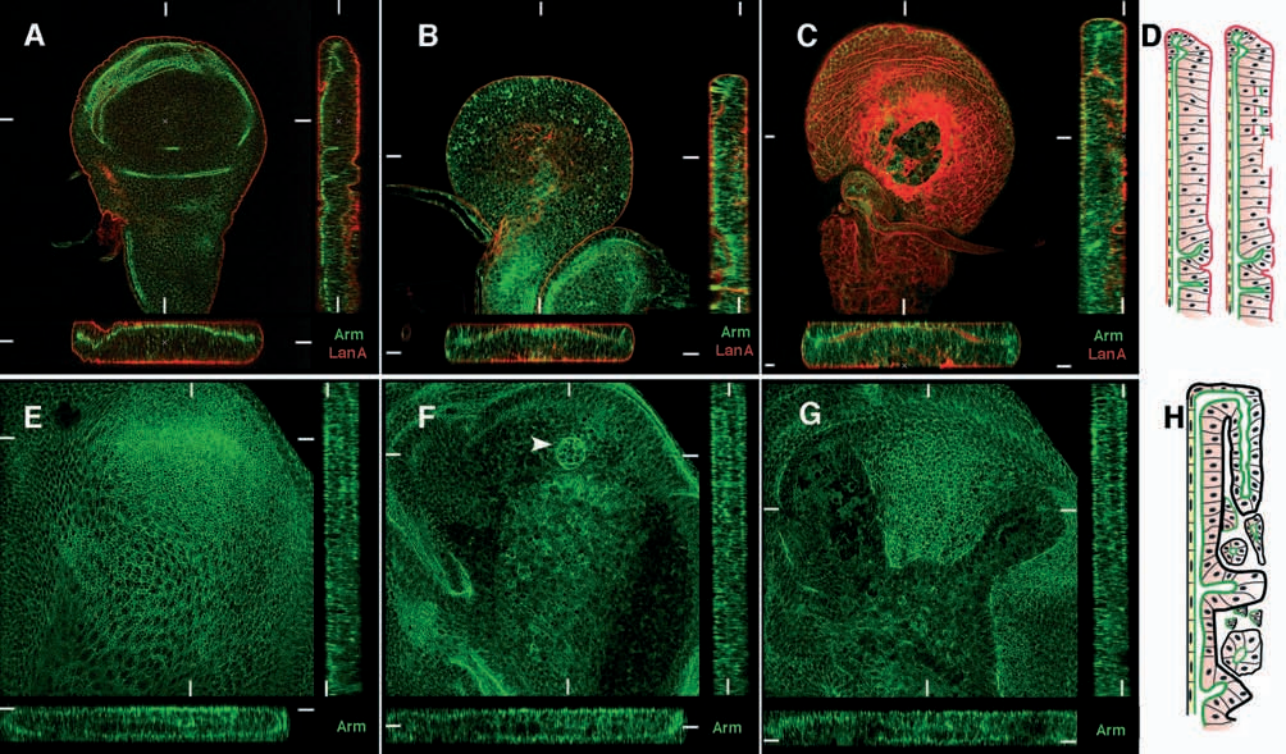
A
B
C
D
Arm
LanA
Arm
LanA
Arm
LanA
E
F
G
H
Arm
Arm
Arm

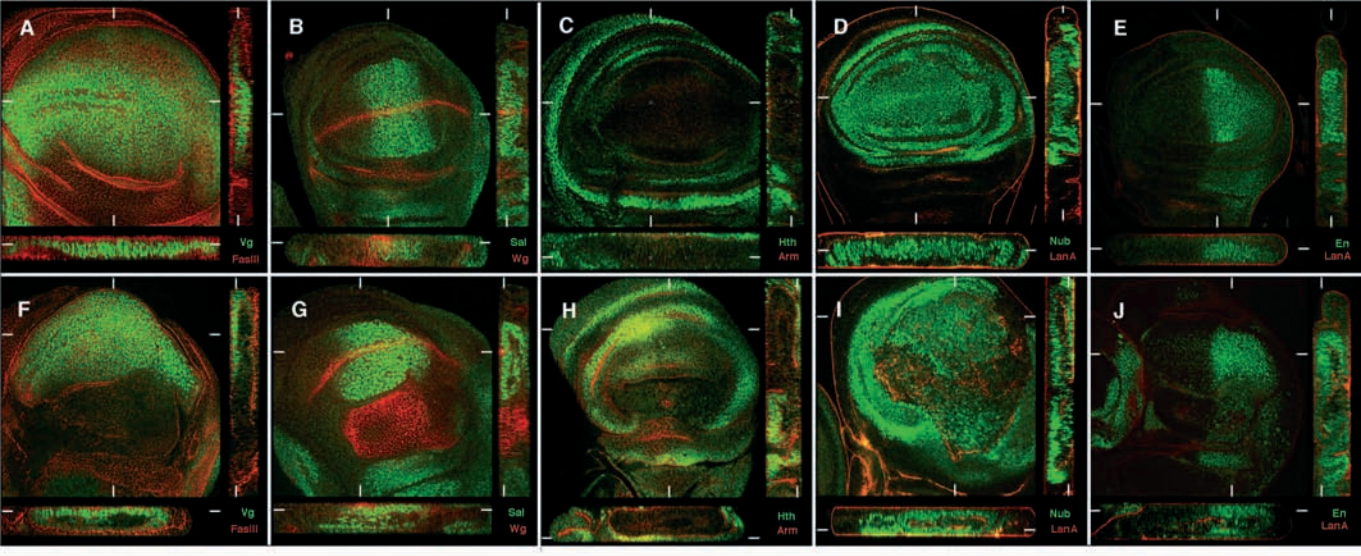
A
Vg
FasIII
B
Sal
Wg
C
Hth
Arm
D
Nub
LanA
E
En
LanA
F
Vg
FasIII
G
Sal
Wg
H
Hth
Arm
I
Nub
LanA
J
En
LanA

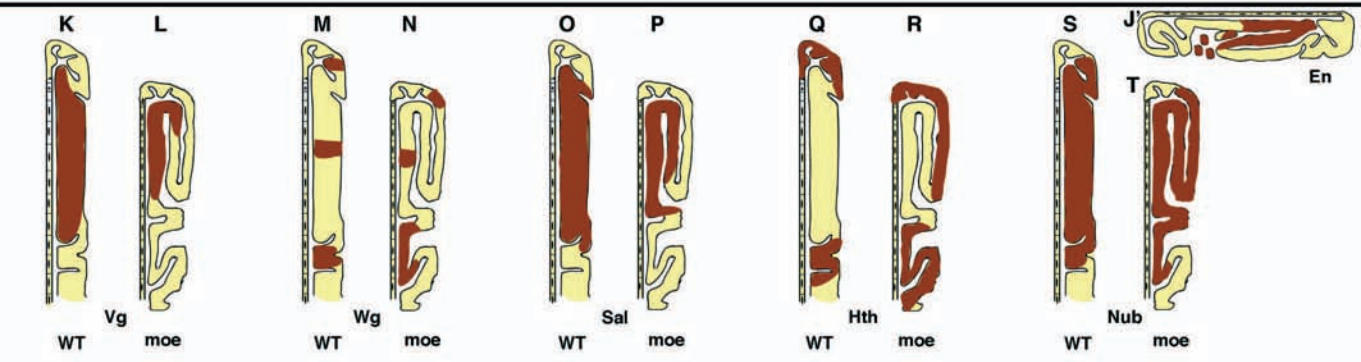
K
L
Vg
WT
moe
M
N
Wg
WT
moe
O
P
Sal
WT
moe
Q
R
Hth
WT
moe
S
T
Nub
WT
moe
J'
En

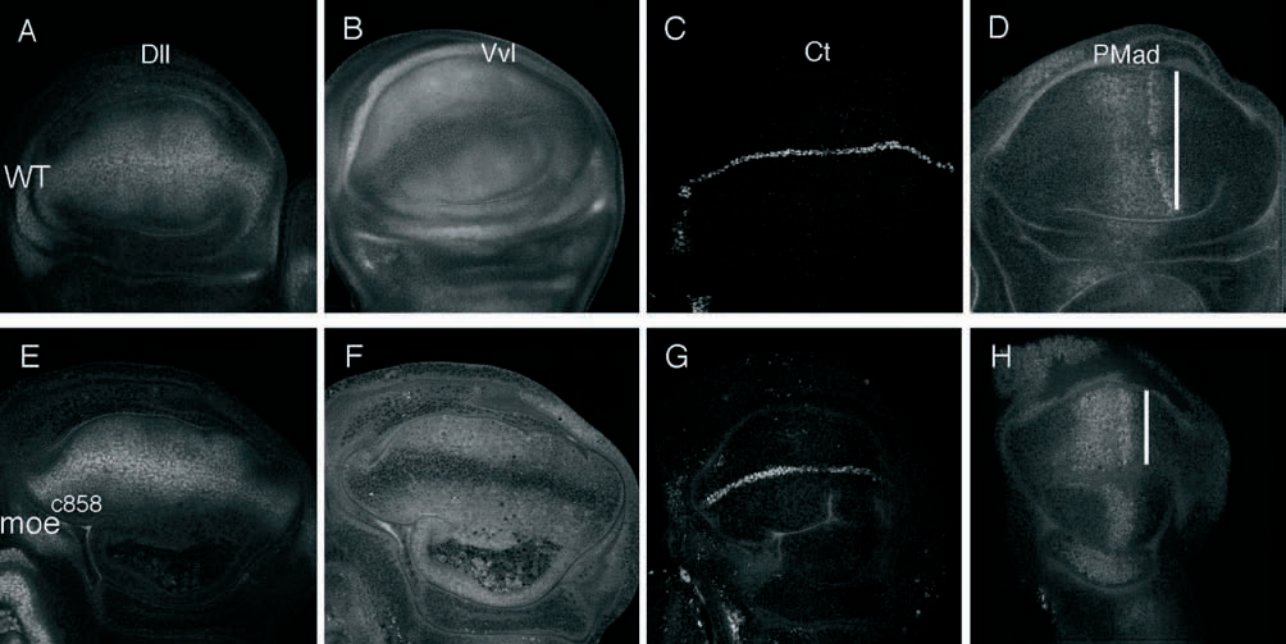
A
Dll
WT
B
Vvl
C
Ct
D
PMad
E
moe
c858
F
G
H

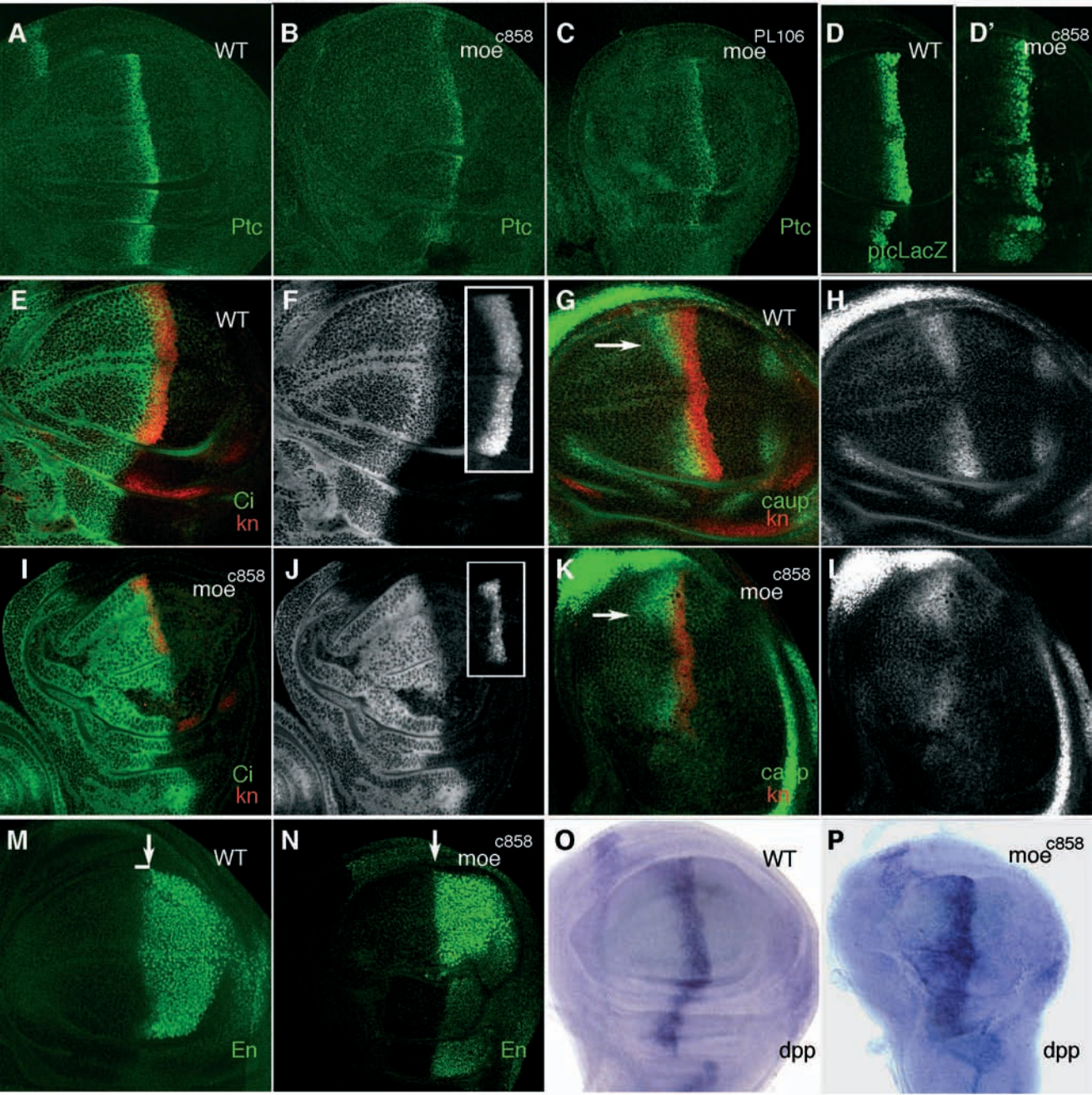
A
WT
Ptc
B
moe c858
Ptc
C
moe PL106
Ptc
D
WT
ptcLacZ
D'
moe c858
E
WT
Ci
kn
F
G
WT
caup
kn
H
I
moe c858
Ci
kn
J
K
moe c858
caup
kn
L
M
WT
En
N
moe c858
En
O
WT
dpp
P
moe c858
dpp

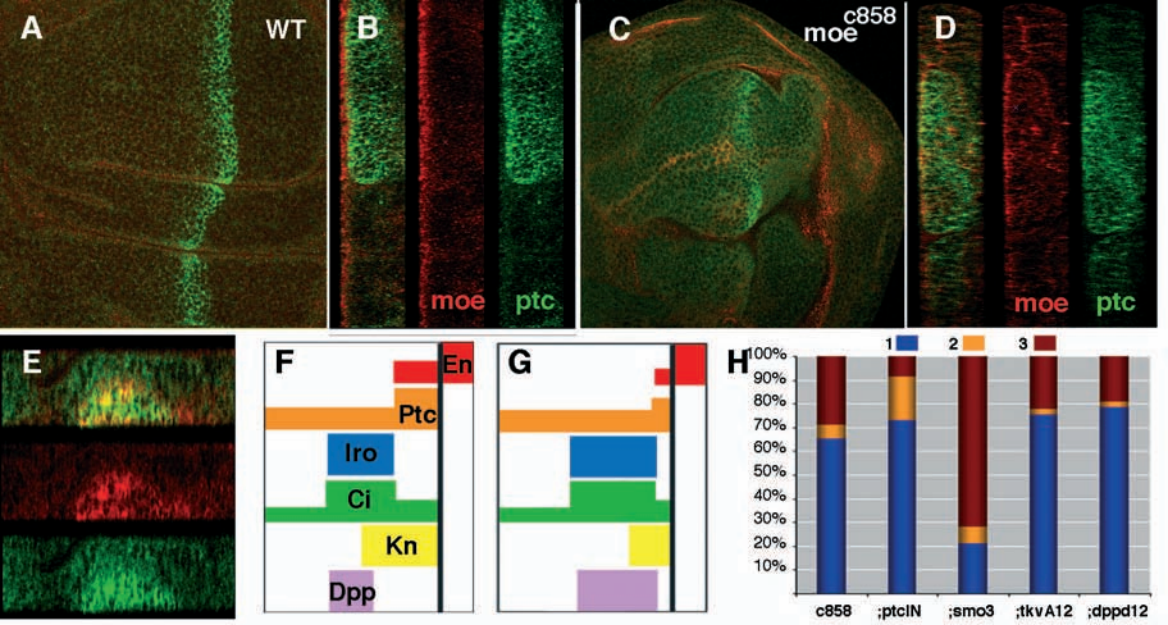
A
WT
B
moe
ptc
C
moe c858
D
moe
ptc
E
F
En
Ptc
Iro
Ci
Kn
Dpp
G
H
1
2
3
100%
90%
80%
70%
60%
50%
40%
30%
20%
10%
c858
;ptcIN
;smo3
;tkvA12
;dppd12

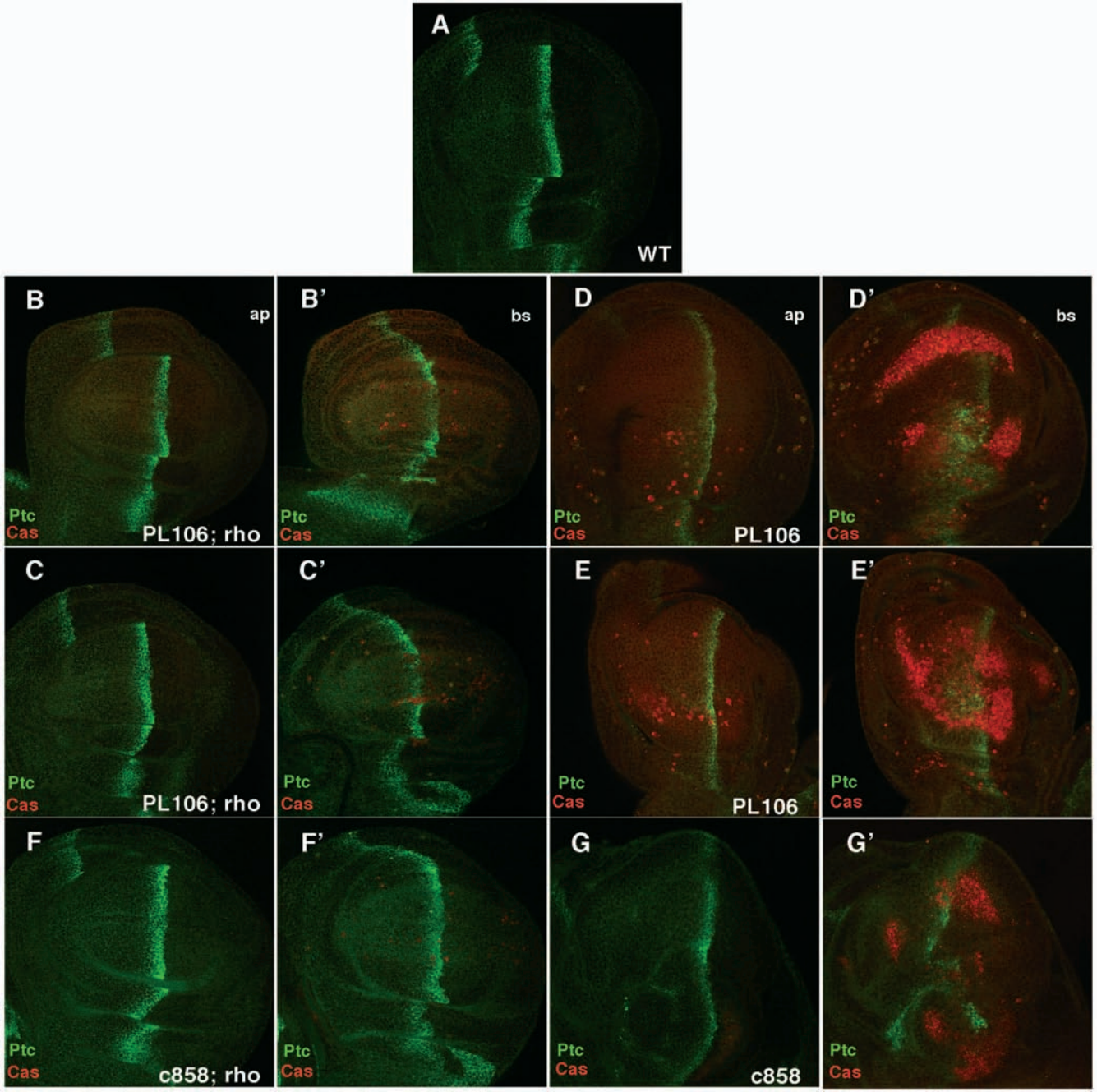
A
WT
B
ap
Ptc
Cas
PL106; rho
B'
bs
Ptc
Cas
D
ap
Ptc
Cas
PL106
D'
bs
Ptc
Cas
C
Ptc
Cas
PL106; rho
C'
Ptc
Cas
E
Ptc
Cas
PL106
E'
Ptc
Cas
F
Ptc
Cas
c858; rho
F'
Ptc
Cas
G
Ptc
Cas
c858
G'
Ptc
Cas

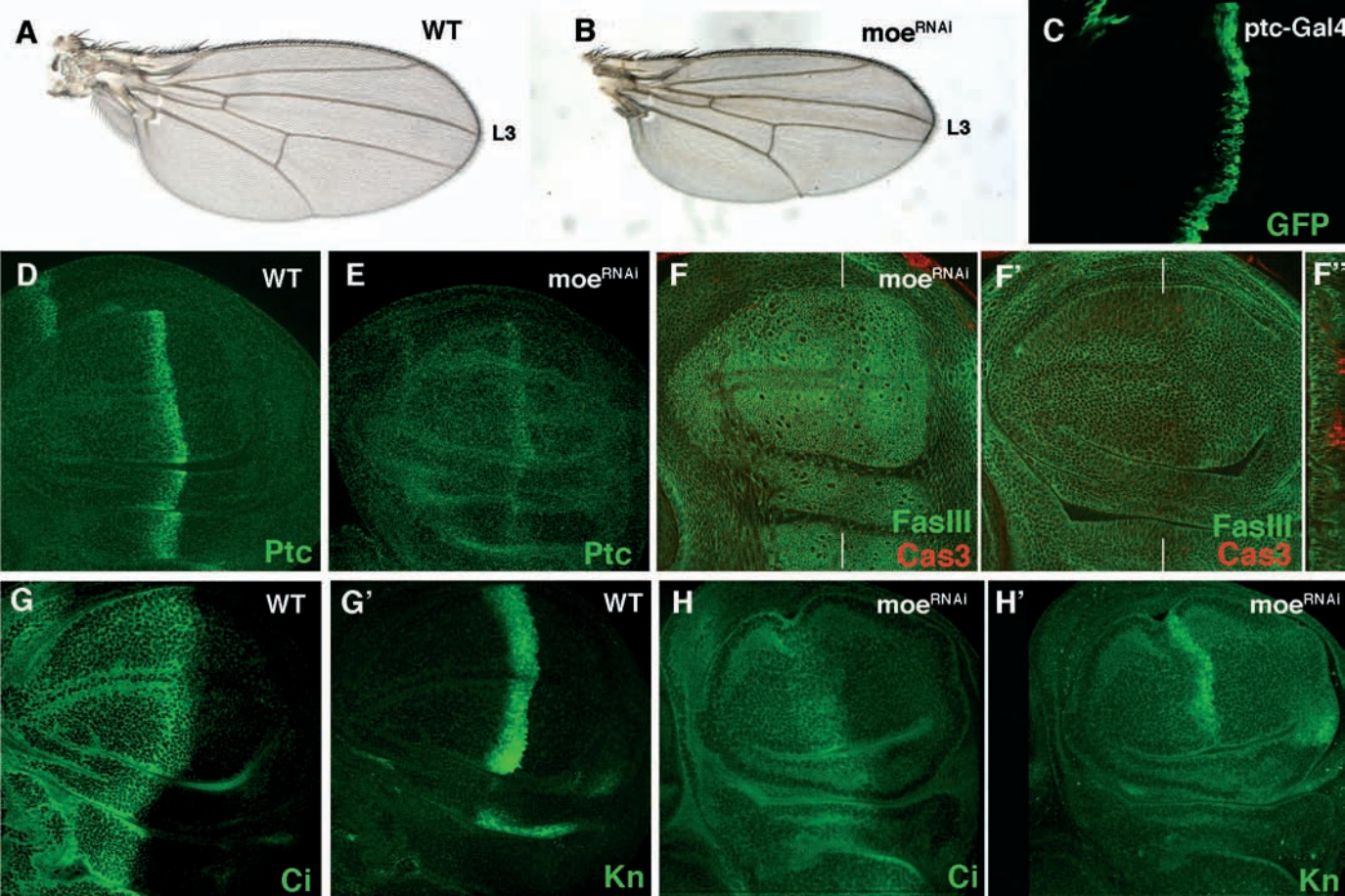
A
WT
L3
B
moeRNAi
L3
C
ptc-Gal4
GFP
D
WT
Ptc
E
moeRNAi
Ptc
F
moeRNAi
FasIII
Cas3
F'
FasIII
Cas3
F''
G
WT
Ci
G'
WT
Kn
H
moeRNAi
Ci
H'
moeRNAi
Kn

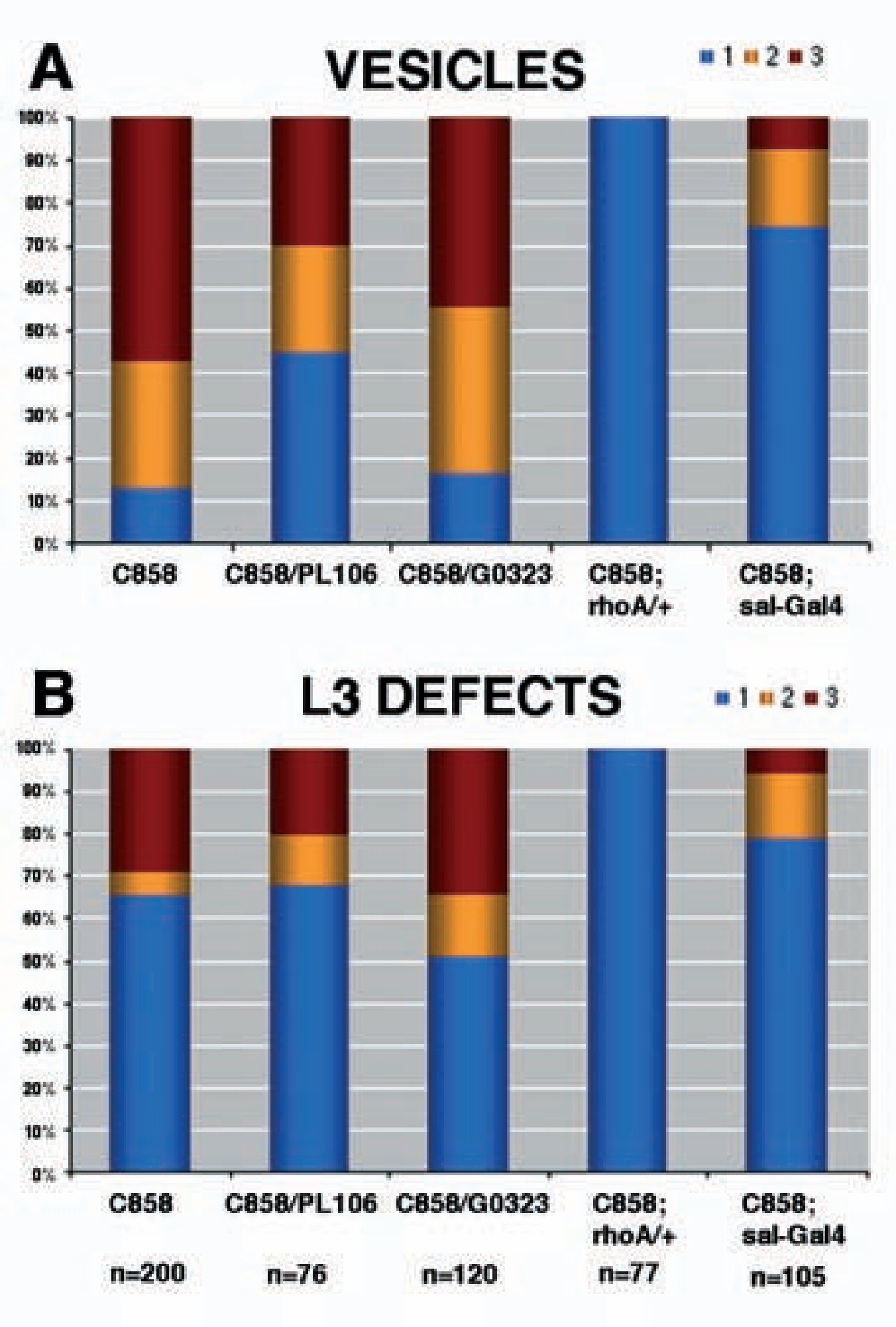
A
VESICLES
1 2 3
100%
90%
80%
70%
60%
50%
40%
30%
20%
10%
0%
C858
C858/PL106
C858/G0323
C858; rhoA/+
C858; sal-Gal4
B
L3 DEFECTS
1 2 3
100%
90%
80%
70%
60%
50%
40%
30%
20%
10%
0%
C858
C858/PL106
C858/G0323
C858; rhoA/+
C858; sal-Gal4
n=200
n=76
n=120
n=77
n=105